# INVESTIGATION OF THE BIOLOGICAL ROLE OF MOUSE ACYLNEURAMINYL HYDROLASE ENZYMES IN THE REGULATION OF NEUROINFLAMMATION

**A Thesis Submitted to**
**the Graduate School of Engineering and Sciences of**
**İzmir Institute of Technology**
**in Partial Fulfillment of the Requirements for the Degree of**

**MASTER OF SCIENCE**

**in Molecular Biology and Genetics**

**by**
**Doğa TABAKACILAR**

**June 2022**
**İZMİR**

# ACKNOWLEDGMENTS

Firstly, I would like to express my deepest gratitude to my supervisor Prof. Dr. Volkan SEYRANTEPE for his encouragement and guidance during my thesis studies. I am very lucky to have him as a mentor as he shared his invaluable experience with me.

I cannot express my gratitude enough to Dr. Seçil AKYILDIZ DEMİR who also mentored and motivated me throughout my studies and shared her expert knowledge.

I am extremely grateful to my thesis committee members Assoc. Prof. Dr. Gülistan MEŞE ÖZÇİVİCİ and Prof. Dr. Kemal Sami KORKMAZ for generously sharing their invaluable advice and guidance.

Many thanks to The Scientific and Technological Research Council of Turkey (TUBITAK) as they supported me with the 2210/A National MSc/MA Scholarship.

I would like to extend my sincere thanks to my colleagues and the undergraduate students in Seyrantepe Lab for their help and support. The warm working environment they provided motivated me during my thesis study. I also would like to thank our veterinarian Güzin SAVRAN İPLİKÇİ for her help and support.

I would like to express my deepest appreciation to my loving parents Füsun TABAKACILAR and Mehmet TABAKACILAR and my beloved friends; Ezgi KESKİN TALDARİ, İrem KAYA, Tuğçe ÇİMEN, Rana ÖZCAN, Melis KONNO, and Fatma SERT for their invaluable support and encouragement.

Lastly, I would like to thank my cats Milka and Mars for keeping me company and entertaining me by just being adorable.

Doğa TABAKACILAR

June 28, 2022

# ABSTRACT

## INVESTIGATION OF THE BIOLOGICAL ROLE OF MOUSE ACYLNEURAMINYL HYDROLASE ENZYMES IN THE REGULATION OF NEUROINFLAMMATION

Sialidosis is a lysosomal storage disorder, and it is inherited by autosomal recessive mutations in the Neuraminidase 1 (NEU1) gene. Neuraminidases or sialidases are catalytic enzymes that carry out the desialylation of glycoconjugates. Deficiencies of neuraminidases lead to the accumulation of sialoglycoconjugates in membranes of cells. Neuroinflammation and neurodegeneration are present in some lysosomal storage diseases such as Tay-Sachs. However, in the sialidosis mouse model, neuroinflammation was never studied. In this study, we investigated the effect of neuraminidase 1, neuraminidase 3, and their combined deficiency on neuroinflammation by using *Neu1*$^{-/-}$, *Neu3*$^{-/-}$ knockout, and *Neu1*$^{-/-}$ *Neu3*$^{-/-}$ double knockout mouse models. *Neu1*$^{-/-}$ *Neu3*$^{-/-}$ knockout mouse model was smaller in comparison to its littermates and showed muscle weakness, tremoring, and 2-3 weeks of a lifetime. Some of the *Neu1*$^{-/-}$ *Neu3*$^{-/-}$ mice died prematurely. To unravel the pathology immunohistochemical, biological, and chromatographic techniques were used. The expression of inflammatory cytokines was altered in the *Neu1*$^{-/-}$, *Neu3*$^{-/-}$, and *Neu1*$^{-/-}$ *Neu3*$^{-/-}$ mice with respect to the brain section. *Neu1*$^{-/-}$ *Neu3*$^{-/-}$ mice showed generally the highest expression of cytokines in the cerebellum compared to the cortex. Neuronal loss was observed in the *Neu1*$^{-/-}$ *Neu3*$^{-/-}$ mice in the cortex, thalamus, and cerebellum. The most remarkable change was in the ganglioside expression pattern in the *Neu1*$^{-/-}$ *Neu3*$^{-/-}$ mice cortex. GD3 expression was present in the cortex of *Neu1*$^{-/-}$ *Neu3*$^{-/-}$ mice where expression of this ganglioside is related to neuroinflammation, neurodegenerative stimuli, autophagosome remodeling and programmed cell death.

**Keywords:** Neuroinflammation, Sialidosis, Neuraminidase, Sialidase, Disease Pathology, NEU1, NEU3, Double Knockout, Transgenic Mouse Models

# ÖZET

## FARE ASİLNÖRAMİNİL HİDROLAZ ENZİMLERİNİN NÖROİNFLAMASYONUN DÜZENLENMESİNDEKİ BİYOLOJİK ROLÜNÜN ARAŞTIRILMASI

Sialidoz bir lizozomal depo bozukluğudur ve kalıtımı Neuraminidase 1 (NEU1) genindeki otozomal resesif mutasyonlarla sağlanır. Nöraminidazlar veya sialidazlar, glikokonjugatların desialilasyonunu gerçekleştiren katalitik enzimlerdir. Nöraminidazların eksiklikleri, hücre zarlarında sialoglikokonjugatların birikmesine yol açar. Literatürde Tay-Sachs gibi bazı lizozomal depo hastalıklarında nöroinflamasyon ve nörodejenerasyon görüldüğüne dair çalışmalar vardır. Fakat, siyalidoz fare modelinde, nöroinflamasyon hiçbir zaman çalışılmamıştır. Bu çalışmada, *Neu1*$^{-/-}$, *Neu3*$^{-/-}$ nakavt, ve *Neu1*$^{-/-}$ *Neu3*$^{-/-}$ çift nakavt fare modelleri kullanılarak nöraminidaz 1, nöraminidaz 3 ve bu enzimlerin kombine eksikliğinin nöroinflamasyon üzerindeki etkisini araştırılmıştır. *Neu1*$^{-/-}$ *Neu3*$^{-/-}$ knockout fare modeli, kafesteki kardeşlerine kıyasla daha küçük bir dış görünüş ve kas zayıflığı, titreme ve 2-3 haftalık bir yaşam süresi göstermiştir. *Neu1*$^{-/-}$ *Neu3*$^{-/-}$ çift nakavt farelerinden bazılarında erken ölüm gözlemlenmiştir. Bu çalışmada, patolojiyi araştırmak için immünohistokimyasal, biyolojik ve kromatografik teknikler kullanıldı. Enflamatuvar sitokinlerin ekspresyonu, *Neu1*$^{-/-}$, *Neu3*$^{-/-}$ ve *Neu1*$^{-/-}$ *Neu3*$^{-/-}$ farelerinde beyin anatomisine göre farklılıklar göstermiştir. *Neu1*$^{-/-}$ *Neu3*$^{-/-}$ farelerinin, kortekse kıyasla genellikle beyincikte en yüksek sitokin ekspresyonunu gösterdiği gözlemlenmiştir. Ek olarak, *Neu1*$^{-/-}$ *Neu3*$^{-/-}$ farelerinde korteks, talamus ve beyincikte nöron kaybı tespit edilmiştir. En dikkat çekici değişiklik, *Neu1*$^{-/-}$ *Neu3*$^{-/-}$ fare korteksindeki gangliosid ekspresyonunda görülmüştür. Nöroinflamasyon, nörodejeneratif uyaranlar, otofagozom modellenmesi ve programlanmış hücre ölümü ile ilişkilendirilmiş GD3 gangliositinin ekspresyonu, *Neu1*$^{-/-}$ *Neu3*$^{-/-}$ farelerinin korteksinde tespit edilmiştir.

**Anahtar Kelimeler:** Nöroinflamasyon, Sialidoz, Nöraminidaz, Sialidaz, Hastalık Patolojisi, NEU1, NEU3, Çift Nakavt, Transgenik Fare Modelleri

# TABLE OF CONTENTS

# LIST OF FIGURES

# LIST OF TABLES

**Table** **Page**

*Dedicated to female scientists*

# CHAPTER 1

# INTRODUCTION

## 1.1. Glycans

There are complex carbohydrates that are mostly located in the plasma membrane. The complex carbohydrates are more recently known as “glycans” (Schnaar, Gerardy-Schahn, and Hildebrandt 2014; Brandley and Schnaar 1986; Reily et al. 2019). The building block of glycans is modified monosaccharides. Acetylation, methylation, sialylation, and sulfation of the monosaccharides lead to the formation of diverse structures and characteristics of glycans (Bhavanandan and Gowda 2014).

The addition of monosaccharides to proteins or lipids is called “glycosylation” (Reily et al. 2019). Glycosylation of the proteins gives rise to the two glycan subcategories: N-glycans and O- glycans. O-glycans are formed by a glycosidic bond between hydroxyl groups of monosaccharides and hydroxyl groups of a protein’s serine or threonine residues (Bhavanandan and Gowda 2014). N-glycans are complex carbohydrates that have a pentasaccharide structure involving 3 mannose and 2 N-acetyl-D-glucosamine (GlcNAc) residues attached to proteins by asparagine (Asn) residues (Bhavanandan and Gowda 2014).

### 1.1.1. Sialic Acids (Neuraminic Acids)

The specific function of a glycan is determined by the monosaccharide that the glycan terminated with (Schnaar, Gerardy-Schahn, and Hildebrandt 2014). Sialic acids are one of the most common monosaccharides that are attached to the end of the glycan chains of N-glycans, O-glycans, and glycosphingolipids (Figure 1.2) (Varki and Schauer 2009; Schnaar, Gerardy-Schahn, and Hildebrandt 2014). The acetylation of the 5-amino-3,5-dideoxy-D-nonulosonic acid which is a monosaccharide of 9 carbons leads to the formation of N-acetylneuraminic acid (NANA, NeuAc) where glycolylation of the monosaccharide acid leads to the formation of N-glycolylneuraminic acid (NeuGc)

(Bhavanandan and Gowda 2014). Modification (e.g., acetylation) of these resulting acids NeuAc and NeuGc give rise to the sialic acid family where more than 50 members are known (Bhavanandan and Gowda 2014; Varki and Schauer 2009). Humans do not utilize NeuGc due to a mutation in the Cytidine-5'-monophospho-N-acetylneuraminic acid (CMP-NeuAc) hydroxylase gene and other mammals that are able to synthesize NeuGc, suppress the expression of NeuGc in their nervous tissue (Suzuki 2006).

The binding of sialic acids to their acceptor glycoconjugate is carried out by the enzymes called sialyltransferases (STs) (Schnaar, Gerardy-Schahn, and Hildebrandt 2014). More than 20 sialyltransferases are known and they are subdivided into four categories according to their glycosidic bond formation type: ST3Gal, ST6Gal, ST6GalNAc, and ST8Sia where they form α2-3, α2-6, or α2-8 bonds between sialic acids and glycoconjugates (Schnaar, Gerardy-Schahn, and Hildebrandt 2014). The removal of sialic acid residues is catalyzed by the sialidase (neuraminidase) family.

## 1.2. Glycoconjugates in Eukaryotes

Glycosylation leads to the formation of glycoconjugates. Glycoconjugates are known as proteins or lipids that are covalently linked to complex glycans. Various glycoconjugates are located at the cell surface in eukaryotes and they can be further divided into three categories: glycoproteins, glycolipids, and proteoglycans (Schnaar, Gerardy-Schahn, and Hildebrandt 2014). Figure 1.1. illustrates the glycoconjugates residing in the extracellular space.

The glycoconjugates at the extracellular space of a cell form a coat that is known as glycocalyx (Figure 1.2.) where the coat encompasses the cell membrane of all cells (Möckl 2020). The glycocalyx is a fundamental structure that has vital roles in cell-cell interactions, embryogenesis, modulating the permeability of the blood-brain barrier, and adhesion of the adaptive immune system cells and nerve cells (Puchwein-Schwepcke, Genzel-Boroviczény, and Nussbaum 2021; Jin et al. 2021; Crocker, Paulson, and Varki 2007; Brandley and Schnaar 1986).

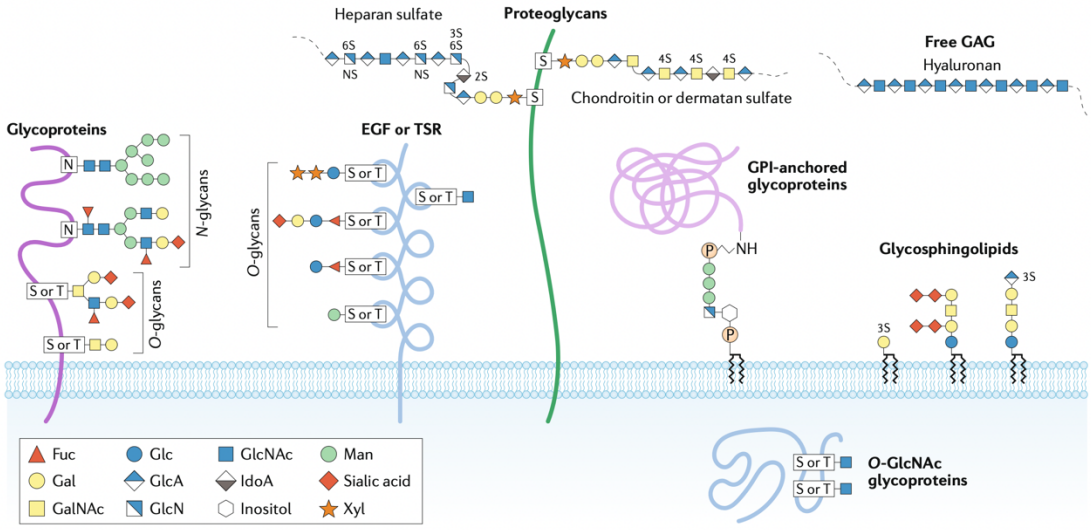


Figure 1. 1. Glycan moieties at the extracellular space

Source: (Reily et al. 2019)

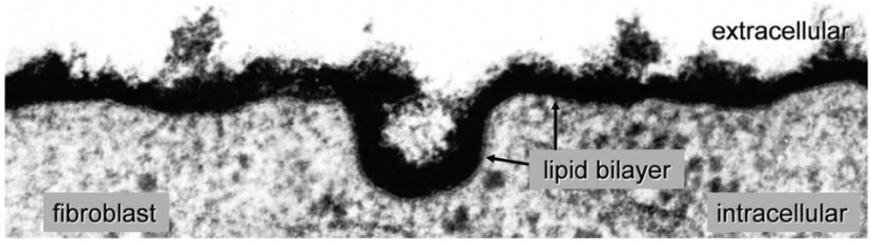


Figure 1. 2. The glycocalyx.

Source: (Schnaar, Gerardy-Schahn, and Hildebrandt 2014)

Phospholipids at the cell membrane allow the maximum number of hydrophobic interactions where negatively charged ions provide space for maximum hydrophilic interactions by attracting water molecules (Singer and Nicolson 1972). Therefore, glycans are selected by evolution to be located predominantly at the glycocalyx due to their negatively charged and unique structure that is sensitive to the slightest change and hydrophilic nature that allows them to expand into the extracellular space (Schnaar, Gerardy-Schahn, and Hildebrandt 2014).

### 1.2.1. Glycosphingolipids

Glycolipids are formed by the addition of glycans to lipids and are mostly comprised of a glycolipid subclass called glycosphingolipids (Schnaar and Kinoshita 2015). Glycosphingolipids are abundantly encountered in cell membranes as a lipid raft constituent from simple organisms to much more complex organisms such as humans (Kopitz 2017; Schnaar and Kinoshita 2015). They take part in the initiation of signal transduction and cell adhesion (Kopitz 2017). The backbone of glycosphingolipids is either lipid moieties sphingosine or ceramide which is attached to a glycan (Yu et al. 2011). The glycan residues determine the function of the glycosphingolipid (Kopitz 2017). Their simplest structure is based on a linkage between ceramide and a monosaccharide galactose (Schnaar and Kinoshita 2015).

Glycosphingolipids are characterized by their core carbohydrate structure as; globoside, isogloboside, ganglioside, isoganglioside, lactoside, neolactoside, lactoganglioside, mucoside, galaside, neogalaside, molluside, arthroside, schistoside, and spirometoside (Yu et al. 2011). Common core structures of glycosphingolipids are depicted in Figure 1.3.

| Root | Structure | Trivial name | Symbol | Sequence * |
|---|---|---|---|---|
| Globo (Gb) | Galα1 → 4Galβ1 → 4GlcCer | Globotriaosylceramide | $GbOse_3Cer$ | |
| | GalNAcβ1 → 3Galα1 → 4Galβ1 → 4GlcCer | Globotetraosylceramide | $GbOse_4Cer$ | |
| Isoglobo (iGb) | Galα1 → 3Galβ1 → 4GlcCer | Isoglobotriaosylceramide | $iGbOse_3Cer$ | |
| | GalNAcβ1 → 3Galα1 → 3Galβ1 → 4GlcCer | Isoglobotetraosylceramide | $iGbOse_4Cer$ | |
| Muco (Mc) | Galβ1 → 4Galβ1 → 4GlcCer | Mucotriaosylceramide | $McOse_3Cer$ | |
| | Galβ1 → 3Galβ1 → 4Galβ1 → 4GlcCer | Mucotetraosylceramide | $McOse_4Cer$ | |
| Lacto (Lc) | GlcNAcβ1 → 3Galβ1 → 4GlcCer | Lactotriaosylceramide | $LcOse_3Cer$ | |
| | Galβ1 → 3GlcNAcβ1 → 3Galβ1 → 4GlcCer | Lactotetraosylceramide | $LcOse_4Cer$ | |
| Neolacto (nLc) | Galβ1 → 4GlcNAcβ1 → 3Galβ1 → 4GlcCer | Neolactotetraosylceramide | $nLcOse_4Cer$ | |
| Ganglio (Gg) | GalNAcβ1 → 4Galβ1 → 4GlcCer | Gangliotriaosylceramide | $GgOse_3Cer$ | |
| | Galβ1 → 3GalNAcβ1 → 4Galβ1 → 4GlcCer | Gangliotetraosylceramide | $GgOse_4Cer$ | |
| Gala (Ga) | Galα1 → 4GalCer | Galabiosylceramide | $GaOse_2Cer$ | |
| | Galα1 → 4Galα1 → 4GalCer | Galatriaosylceramide | $GaOse_3Cer$ | |

Figure 1. 3. Common core structures of glycosphingolipids

Source: (Kopitz 2017)

The dynamic and flexible structure of the cell membranes is dependent on the de novo biosynthesis of glycoconjugates. Glycosphingolipids undergo degradation and

synthesis with a rapid turnover rate. In non-dividing cells, cell surface degradation halftime is 1 hour (Tettamanti 2004).

### 1.2.2. Gangliosides

Gangliosides are the glycosphingolipid class that is abundant in the brain and are involved in various cellular processes such as cell-cell interaction (Yu et al. 2011). They contain sialic acid residues bound to the inner galactose within their ceramide-tailed structure (Sipione et al. 2020). Gangliosides that contain zero sialic acid residues are known as “asialo-series gangliosides”, one sialic acid residue as “a-series gangliosides”, two sialic acid residues as “b-series gangliosides”, and three sialic acid residues as “c-series gangliosides” (Yu et al. 2011).

Gangliosides mostly reside in the extracellular part of the cell membrane and in the nuclear membrane. They are also found in microdomains of plasma membranes such as lipid rafts and caveolae (Yu et al. 2011).

Gangliosides are mostly synthesized by the addition of sialic acid residues to LacCer. However, there are also gangliosides synthesized from another glycosphingolipid known as GalCer (Yu et al. 2011). GA2, GA1, GM1b, and GD1c are a member of the asialo-series gangliosides whereas GM3, GM2, GM1 GD1a, and GT1a are a-series gangliosides, GD3, GD2, GD1b, GT1b, GQ1b are b-series gangliosides and GT3, GT2, GT1c, GQ1c, and GP1c are c-series gangliosides (Yu et al. 2011).

In a differentiating neuron, the number of gangliosides increases until it fully differentiates (Prinetti et al. 2001). In the embryonic brain of wild-type mice, GM3 and GD3 gangliosides are abundant whereas in the adult brain 97% of the gangliosides are GM1, GD1a, GD1b, and GT1b (Yu et al. 1988; Ngamukote et al. 2007).

Besides contributing to the cellular interactions, gangliosides participate in various processes. By forming a complex with myelin-associated glycoprotein (MAG), GD1a and GT1b gangliosides are involved in the protection and regeneration of axons and also in the intercommunication between axons and myelin (Yang et al. 1996; Pshezhetsky and Ashmarina 2018). GD3 ganglioside is involved in the preservation of the stem cell niche in the brain and induction of neurogenesis by interacting with epidermal growth factor receptor (EGFR) (Wang and Yu 2013; Pshezhetsky and Ashmarina 2018). On the other hand, the accumulation of GD3 ganglioside is observed

in the cells that are undergoing apoptosis through death receptor activation (Garofalo et al. 2015).

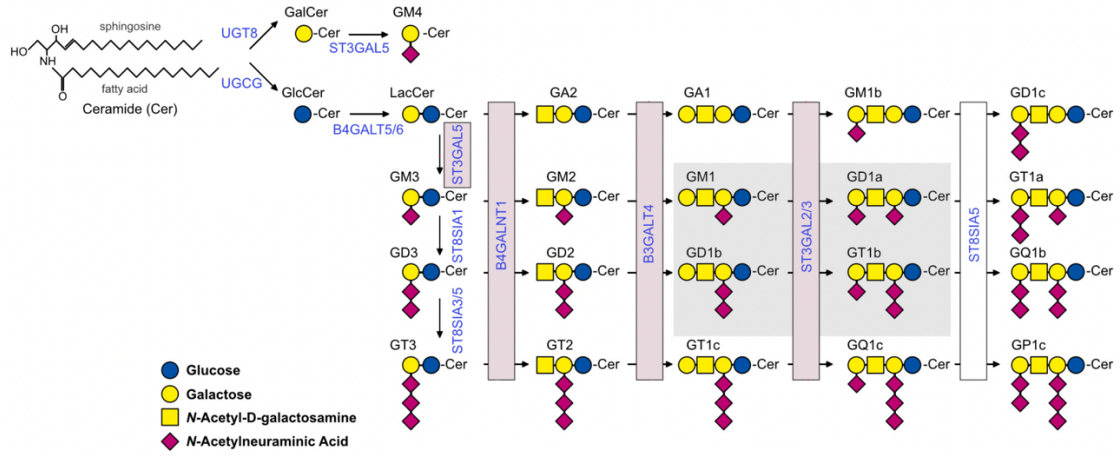


Figure 1. 4. The ganglioside biosynthesis

Source: (Sipione et al. 2020)

The gangliosides are synthesized in Golgi and ER (Kolter, Proia, and Sandhoff 2002) and recycled from the plasma membrane to initiate de novo ganglioside biosynthesis (Tettamanti 2004). The mechanism of ganglioside biosynthesis is illustrated in Figure 1.4.

Endo/lysosomal network participates in the de novo synthesis of gangliosides. The turnover rate of the de novo biosynthesis is dependent on a number of concepts: the enzymes involved in the metabolic pathway, an external signal that initiates the degradation of the gangliosides, endo/lysosomal metabolic flux, and the nature of the cell as dividing or nondividing (Tettamanti 2004).

The degradation of the gangliosides is catalyzed by neuraminidase 1-4, and glycosidases (Figure 1.5). Glycosidases cooperate with protein cofactors known as sphingolipid activator proteins Saposins A, B, C, D and GM2 activator protein (GM2Ap) (Li et al. 2001).

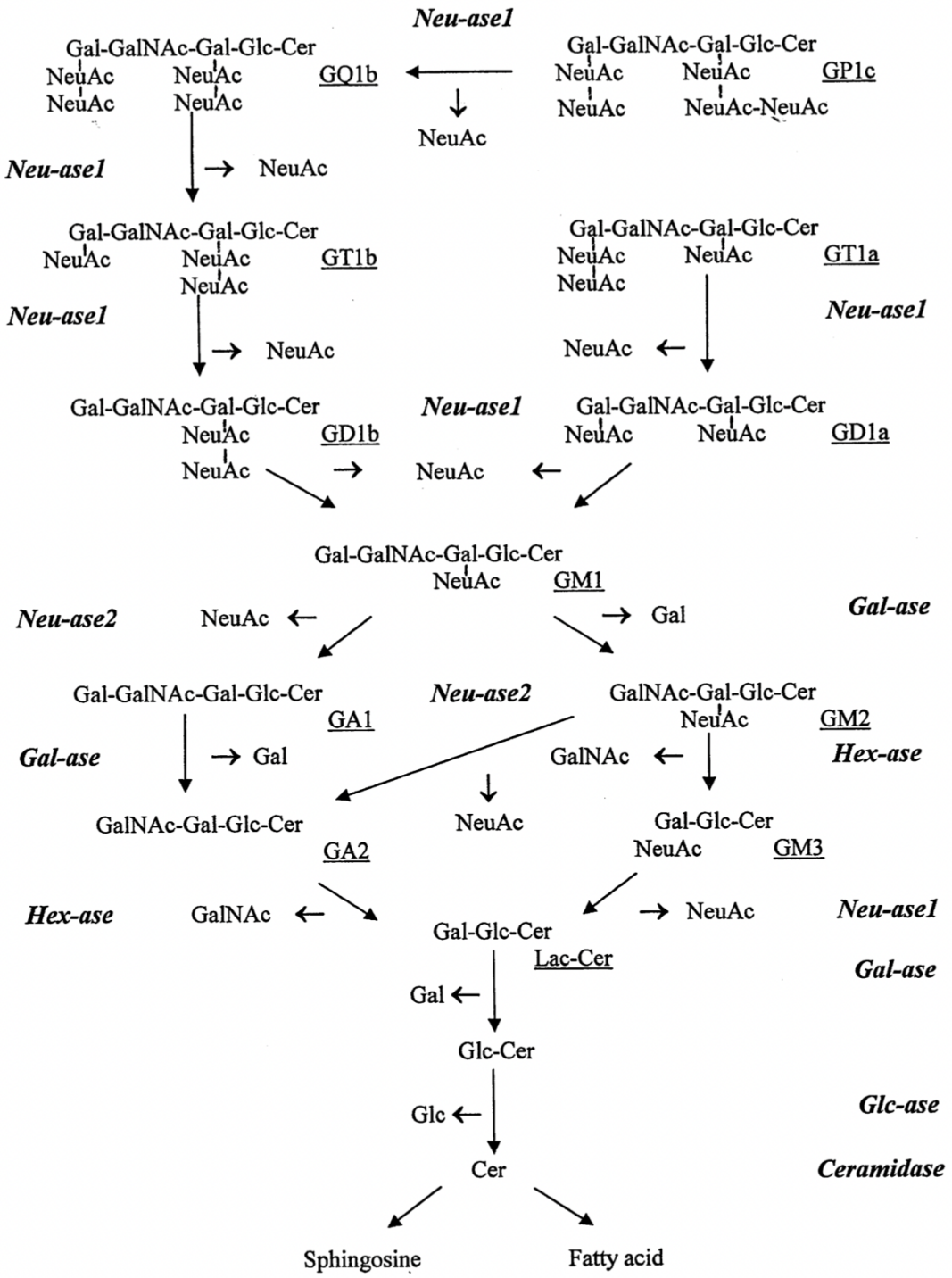


Figure 1. 5. The ganglioside degradation pathway

Source: (Tettamanti 2004)

NEU1 and NEU3 sialidases can degrade GM2 and GM3 into asialo glycosphingolipids (Seyrantepe et al. 2003). Removal of galactose residues from GM1 is

catalyzed by β-galactosidase enzyme (O'Brien 1975). The conversion of GM3 to LacCer is carried out by NEU3 (Monti et al. 2010). GM2 to GM3 conversion is catalyzed by β-N-acetylhexosaminidase A (Hex A), and GM2AP (Li et al. 2001). The sialidase NEU3 catalyzes the removal of sialic acid residues from GM2. The resulting ganglioside GA2 from this reaction is further hydrolyzed by the enzyme β-N-acetylhexosaminidase B (Hex B) into sphingolipid derivatives (Demir et al. 2020; Yuziuk et al. 1998).

## 1.3. Neuraminidases

Neuraminidases or sialidases remove terminal sialic acid residues from glycoconjugates. There are four major families of neuraminidases found in mammalians so far which are NEU1, NEU2, NEU3, and NEU4 (Monti et al. 2010). Neuraminidases are known to be differentially expressed through the development (Hasegawa et al. 2001).

### 1.3.1. NEU1

NEU1 is known as the lysosomal sialidase and it is located at the lysosomal membrane and lumen (Lukong et al. 2001). Activation of NEU1 requires the formation of a multienzyme complex with three other enzymes: Cathepsin A, β-galactosidase, and N-acetylgalactosamine-6-sulfatase (Lukong et al. 2001; Pshezhetsky and Ashmarina 2001; Timur, Demir, and Seyrantepe 2016). The dissociations of these complex inactivate NEU1 (Miyagi and Yamaguchi 2012). NEU1 preferably hydrolyzes the α2-3 and α2-6 glycosidic bonds (Monti et al. 2010). Additionally, NEU1 acts as an integral membrane-bound protein and is transferred into the endo/lysosomal network by an interaction between adaptor protein 3 (AP-3) and a tyrosine-based internalization signal at the C-terminus (Lukong et al. 2001; Monti et al. 2010). In humans, NEU1 is differentially expressed in various organs such as the brain, kidney, liver, testis, and also in cells of the immune system such as macrophages and T cells (Monti et al. 2010). NEU1 has the highest expression among other sialidases, and it is located at chromosome 6p 21.3 in humans (Miyagi and Yamaguchi 2012). In murine species, it is located at chromosome 17 (Miyagi and Yamaguchi 2012).

NEU1 participates in various processes such as the synthesis of IL-4, and IFN-γ (Seyrantepe et al. 2003; Nan, Carubelli, and Stamatos 2007), activation and differentiation of adaptive immune system cells (Landolfi et al. 1985; Seyrantepe et al. 2003; Liang et al. 2006; Stamatos et al. 2010), elastin metabolism (Starcher et al. 2008; Seyrantepe et al. 2008; Bocquet et al. 2021), TLR2, TLR3, and TLR4 activation (Amith et al. 2009), phagocytosis in macrophages (Seyrantepe et al. 2010), immune cell adhesion (Miyagi and Yamaguchi 2012), cancer pathogenesis (Garcia-Dominguez et al. 2022; Lv et al. 2020) and suppression of cancer cell migration and adhesion (Uemura et al. 2009).

### 1.3.2. NEU2

NEU2 is known as the cytosolic sialidase and preferably recognizes the α2-3 glycosidic bonds in oligosaccharides, glycoproteins, and gangliosides (Monti et al. 2010; Miyagi and Yamaguchi 2012). NEU2 can catalyze the sialic acid removal from various glycoconjugates at an almost neutral pH (Miyagi and Yamaguchi 2012). The cytosolic sialidase exhibits low affinity to α2-6 and α2-8 glycosidic bonds present in sialoglycoconjugates (Monti et al. 2010). In humans, NEU2 is expressed much lower than in other neuraminidases and is located at chromosome 2q 37 (Miyagi and Yamaguchi 2012). In murine species, NEU2 is located at chromosome 1 (Miyagi and Yamaguchi 2012). NEU2 participates in muscle and cancer cell differentiation (Monti et al. 2010).

### 1.3.3. NEU3

NEU3 is known as the plasma membrane sialidase due to its cis-acting and trans-acting features that allow the removal of sialic acid residues at the plasma membrane and also in the plasma membrane of neighbor cells (Monti et al. 2010). It recognizes and hydrolyzes the α2-3 and α2-6 glycosidic bond faster than α2-8 bond (Miyagi and Yamaguchi 2012). NEU3 is located at chromosome 11q 13.5 in humans and at chromosome 7 in murine species (Miyagi and Yamaguchi 2012).

NEU3 participates in the regulation and maintenance of membrane microdomains, neuronal cell differentiation, axon growth and regeneration, muscle cell differentiation, and apoptosis (Monti et al. 2010; Miyagi and Yamaguchi 2012).

### 1.3.4. NEU4

NEU4 sialidase catalyzes the removal of sialic acid residues in mitochondria, lysosomal lumen, and endoplasmic reticulum (Seyrantepe et al. 2004; Miyagi and Yamaguchi 2012). Two isoforms of NEU4 exist in humans: long isoform NEU4L localized in mitochondria and short isoform NEU4S localized in internal membranes (Seyrantepe et al. 2004; Monti et al. 2010; Yamaguchi et al. 2005). Both the two isoforms are expressed in muscles, brain, and kidney while NEU4S is mainly expressed in the colon and liver (Lipnicanova et al. 2020).

NEU4 participates in hydrolyzation of mucins (Seyrantepe et al. 2004), neuronal differentiation, apoptosis, and cell adhesion (Miyagi et al. 2018).

## 1.4. Neuroinflammation

Although the brain is included in immune-privileged organs, this does not necessarily indicate that the brain is not capable of manifesting an immune response. A recent study that rediscovered brain meningeal lymphatic vasculature shows that the transportation of antigens and immune cells from the inflamed area of the brain to the nearby lymph node is carried out through this vasculature (das Neves, Delivanoglou, and Da Mesquita 2021).

If neuroinflammation cannot be contained and resolved, it leads to chronic inflammation. During an acute inflammatory response, several changes in the tissue are observed which are increased blood flow to the affected area, vessels becoming more permeable, and leukocyte migration into the tissue (Roitt, Brostoff, and Male 2001). However, inflammation in the brain and spinal cord cannot be consistent and standardized. The immune response differs according to the region that is affected, and the duration, intensity, and timing of the response (Bosch and Kielian 2015). A transient immune response might be neuroprotective while a chronic inflammation in the central nervous system (CNS) could have detrimental effects such as inflammatory mediator and cytokine release, apoptosis-inducing signals, and a neurotoxic environment formation (Bosch and Kielian 2015). Since neurons are in the post-mitotic phase and are not able to divide, such a chronic inflammatory response would be irreversible.

The cells of the nervous system can be divided into two categories: neurons and glial cells. Glial cells comprise astrocytes, oligodendrocytes (macroglia), and microglia. The immune response of the brain is primarily induced by microglia, astrocytes, endothelial cells, and blood-derived monocytes (DiSabato, Quan, and Godbout 2016). The activation of microglia (microgliosis) and astrocytes (astrogliosis) through sensing the damage-associated molecular patterns (DAMPs) or pathogen-associated molecular patterns starts the neuroinflammatory response in the brain (Bosch and Kielian 2015).

Microglia are one of the non-neuronal cell types in the brain which senses stress signals PAMPs and DAMPs released from dying neurons and phagocytose the cell debris. They are derived from myeloid lineage (Chan, Kohsaka, and Rezaie 2007) and express toll-like receptors (TLRs) and pathogen recognition receptors (PRRs) to survey CNS for PAMPS and DAMPs (Lyman et al. 2014; Hanke and Kielian 2011). Microglia releases cytokines and chemokines in order to induce migration of blood circulating leukocytes into the inflamed brain section such as IL-1α, IL-1β, IL-3, IL-5, IL-6, TNF-α (McGeer and McGeer 1995). They also secrete reactive oxygen and nitrogen intermediates (McGeer and McGeer 1995).

Astrocytes together with pericytes, endothelial cells, basement membrane, and glycocalyx construct the blood-brain barrier (Jin et al. 2021). When astrocytes are activated, they also release cytokines like microglia. For instance, they secrete IL-1, IL-6, IL-8, IL-10, IFN-α, IFN-β, TNF-α, TGF-β, CCL2, CCL3, CCL4, CCL5, CCL20, CXCL10, and CXCL12 (Meares and Benveniste 2014). Activated astrocytes are identified by a morphologic change involving increased expression of intermediate filaments: glial fibrillary acidic protein (GFAP) and vimentin (Bosch and Kielian 2015; Meares and Benveniste 2014). In chronic neuroinflammation, neurotrophic support provided by astrocytes to neurons is disrupted (Lee and MacLean 2015).

## 1.5. Lysosomal Storage Diseases

Lysosomal storage diseases (LSD) are characterized by mutations in the genes that disrupt lysosomal homeostasis. In LSDs, the disease pathogenesis is caused by excess storage of glycoconjugates in the lysosomes resulting from deficiencies in the lysosomal enzymatic proteins or lysosomal enzymes (Platt et al. 2018). Nearly all LSDs are inherited autosomal recessively except Fabry and mucopolysaccharidosis (MPS) type II which

exhibit X-linked inheritance (Meikle et al. 1999) and the incidence rate is 1:5000 (Bosch and Kielian 2015; Platt et al. 2018). LSDs are mostly diagnosed in infants or children, but the adult onset of the disease is also present (Platt, Boland, and van der Spoel 2012).

LSDs are named according to the storage molecule and onset of the disease such as congenital, infantile, late-infantile, juvenile, and adult-onset. The onset of the LSD is dependent on the chemical structure of the storage molecule and characteristics of the mutation that is concerning the activity of the mutant protein (Platt et al. 2018).

In almost all LSDs central nervous system (CNS) pathology is present. For example, neurodegeneration and neuroinflammation are observed in some LSDs such as Tay-Sachs (Demir et al. 2020; Seyrantepe et al. 2018), mucopolysaccharidoses I, III, IIIA, IIIB, IIIC, and VII (Ohmi et al. 2003; Wilkinson et al. 2012; Martins et al. 2015; Archer et al. 2014). However, disease prognosis differs related to the affected region of the CNS (Platt, Boland, and van der Spoel 2012). The factors that affect LSD prognosis are the ability of each neuronal population in the CNS to synthesize different amounts of glycoconjugates, sensitivity to storage of a CNS cell in the affected region, and the effect of storage glycoconjugate on the CNS cell (Platt, Boland, and van der Spoel 2012). In general, CNS pathology involving neuroinflammation in LSDs may result from a combined collaboration of cytokines and chemokines released from astrocytes and microglia, the presence of reactive oxygen and nitrogen species, infiltration of leukocytes, innate immune system elements, loss of lysosomal function that leads to the release of lysosomal enzymes into the cytosol, DAMPs released from dying neurons, disruption of glutamate homeostasis, interruption of $Ca^{++}$ homeostasis, abnormal mitochondrial function, increase in the blood-brain barrier permeability, and loss of endoplasmic reticulum function that leads to unfolded protein response (UPR) (Lyman et al. 2014; Meares and Benveniste 2014; Bosch and Kielian 2015; Di Vito, Donato, and Tomassoni 2017; Platt, Boland, and van der Spoel 2012).

### 1.5.1. Sialidosis

Sialidosis is a lysosomal storage disease (LSD) that is very rare and inherited autosomal recessively by mutations in the NEU1 gene located at chromosome 6p21.3. There are 34 mutations identified in the NEU1 gene that causes sialidosis (Seyrantepe et al. 2003).

Sialidosis can be classified into two types according to the onset of the disease: Type I and Type II. In Type I sialidosis where symptoms are manifested in late-onset, the disease progresses in mild conditions. Type I sialidosis is diagnosed by the cherry-red spots in the patients, seizures, overreactive reflexes, ataxia, myoclonus movements, and ophthalmologic symptoms (Seyrantepe et al. 2003). In Type II sialidosis which is the early-onset form of the disease, the symptoms are more severe than in Type I sialidosis. Type II patients suffer from mental defects, visceromegaly, skeletal changes resembling Hurler syndrome (dysostosis multiplex), and sialoglycoconjugates in the urine (Seyrantepe et al. 2003; de Geest et al. 2002).

Neuraminidase 1 is known as the lysosomal sialidase, and these mutations result in the storage of sialoglycoconjugates in the lysosome and cause lysosomal homeostasis disturbance. The disturbance in the lysosomal homeostasis leads to lysosomal function disruption, lipid body generation, disturbance in the lysosomal membrane structure, and finally release of the lysosomal content into cytoplasm such as cathepsins, hydrolases and metabolites (Pereira et al. 2010; Futerman and van Meer 2004). The lysosomes that are deformed by excessive storage can be identified as DAMPs during immune surveillance and lead to the initiation of neuroinflammation (Futerman and van Meer 2004; Platt, Boland, and van der Spoel 2012).

## 1.5.2. Sialidosis Mouse Model

The sialidosis mouse model is created by insertion of LacZ/PGK/neo expression cassette into exon1 of the Neu1 gene (de Geest et al. 2002). *Neu1*$^{-/-}$ mice showed vacuolization in the adaptive immune system cells except for neutrophils (de Geest et al. 2002). The weight of the *Neu1*$^{-/-}$ mice was 25% lighter than their littermates and they were sterile after 10 weeks of age. Additionally, *Neu1*$^{-/-}$ mice exhibit splenomegaly, and bone deformities resembling Type II sialidosis patients (de Geest et al. 2002). The lifetime of *Neu1*$^{-/-}$ mice differs between 8 months and 12 months of age (de Geest et al. 2002).

## 1.6. Aim of the Study

We hypothesize that there is an involvement of the neuroinflammatory modulators in the disease progression of sialidosis since CNS pathology is observed in many LSDs. Thus, the aim of this study is to unravel the effect of lysosomal sialidase neuraminidase 1 and plasma membrane sialidase neuraminidase 3 deficiency in neuroinflammation and elucidate if there is a change in the expression of glycosphingolipid subclass gangliosides in mouse brain. To accomplish that, *Neu1*$^{-/-}$, *Neu3*$^{-/-}$, and *Neu1*$^{-/-}$ *Neu3*$^{-/-}$ mouse models are investigated for the presence of neuroinflammation.

# CHAPTER 2

# MATERIALS AND METHODS

## 2.1. Animals

*Neu1*$^{-/-}$ mice and *Neu3*$^{-/-}$ mice that are used in this study were a kind gift from Dr. Alessandra d'Azzo (Genetics Department, Comprehensive Cancer Center, St. Jude Graduate School of Biomedical Sciences, Tennessee, USA) and Dr. Taeko Miyagi (Miyagi Cancer Center Research Institute, Natori, Japan), respectively.

The transgenic *Neu1*$^{-/-}$ mice are created by insertion of LacZ/PGK/neo expression cassette into exon1 of the Neu1 gene (de Geest et al. 2002). The genetically modified Neu1 gene results in a truncated version of the neuraminidase 1 (de Geest et al. 2002), rendering the gene functionless in mice.

The transgenic *Neu3*$^{-/-}$ mice are generated by insertion of the PGK/neo/bpA and DT-A expression cassettes into exon3 of the Neu3 gene to interfere with the coding region of the gene (Yamaguchi et al. 2012).

*Neu1*$^{-/-}$ *Neu3*$^{-/-}$ mice are bred by crossing *Neu1*$^{+/-}$ mice with *Neu3*$^{-/-}$ mice to generate the heterozygous genotype pups since *Neu1*$^{-/-}$ mice are sterile. Then, the generation inbred with each other to obtain female and male pups that have the following genotype: *Neu1*$^{+/-}$ *Neu3*$^{+/-}$. However, by crossing *Neu1*$^{+/-}$ *Neu3*$^{+/-}$ mice with each other, the probability of producing a pup that has *Neu1*$^{-/-}$ *Neu3*$^{-/-}$ genotype is 1/16. Therefore, mice with *Neu1*$^{+/-}$ *Neu3*$^{-/-}$ genotype are mated with each other to generate desired genotypic characteristics. The probability of obtaining Neu*1*$^{-/-}$ *Neu3*$^{-/-}$ mice with the crossing mentioned earlier is 1/4 which is 4 times higher than 1/16. Table 2.1 illustrates the breeding scheme in detail.

All the mice that are used in this study are housed and maintained at the Izmir Institute of Technology Experimental Animal Facility where animal well-being is considered highly significant. The facility is accredited by the Turkish Council on Animal Care (TCAC). Mice are kept under constant room temperature (25°C) and 12-hour day:12-hour night cycle, complying with regulations of TCAC. As a mating combination, a polygamous trio is chosen, 2 female mice and a male mouse were present per cage.

Table 2. 1 Breeding scheme of $Neu1^{+/-}$ and $Neu3^{-/-}$ mice

| | ♀ | | ♂ |
|---|---|---|---|
| **P** | ***Neu1*$^{+/-}$ *Neu3*$^{+/+}$** | **X** | ***Neu1*$^{+/+}$ *Neu3*$^{-/-}$** |
| 1/2 | *Neu1*$^{+/-}$ *Neu3*$^{+/-}$ | | |
| 1/2 | *Neu1*$^{+/+}$ *Neu3*$^{+/-}$ | | |

| | ♀ | | ♂ |
|---|---|---|---|
| **F1** | ***Neu1*$^{+/-}$ *Neu3*$^{+/-}$** | **X** | ***Neu1*$^{+/-}$ *Neu3*$^{+/-}$** |
| 1/16 | *Neu1*$^{+/+}$ *Neu3*$^{+/+}$ | | |
| 2/16 | *Neu1*$^{+/+}$ *Neu3*$^{+/-}$ | | |
| 1/16 | *Neu1*$^{+/+}$ *Neu3*$^{-/-}$ | | |
| 2/16 | *Neu1*$^{+/-}$ *Neu3*$^{+/+}$ | | |
| 4/16 | *Neu1*$^{+/-}$ *Neu3*$^{+/-}$ | | |
| 2/16 | *Neu1*$^{+/-}$ *Neu3*$^{-/-}$ | | |
| 1/16 | *Neu1*$^{-/-}$ *Neu3*$^{+/+}$ | | |
| 2/16 | *Neu1*$^{-/-}$ *Neu3*$^{+/-}$ | | |
| **1/16** | ***Neu1*$^{-/-}$ *Neu3*$^{-/-}$** | | |

| | ♀ | | ♂ |
|---|---|---|---|
| **F2** | ***Neu1*$^{+/-}$ *Neu3*$^{-/-}$** | **X** | ***Neu1*$^{+/-}$ *Neu3*$^{-/-}$** |
| 1/4 | *Neu1*$^{+/+}$ *Neu3*$^{-/-}$ | | |
| 2/4 | *Neu1*$^{+/-}$ *Neu3*$^{-/-}$ | | |
| **1/4** | ***Neu1*$^{-/-}$ *Neu3*$^{-/-}$** | | |

## 2.2. Genotyping of Mice

The confirmation of the genotypes that *WT*, *Neu1*$^{-/-}$, *Neu3*$^{-/-}$, and *Neu1*$^{-/-}$ *Neu3*$^{-/-}$ mice have was done by applying DNA isolation protocol to 2 mm length clipped tails of the weaned mice and then conducting PCR experiments on the extracted DNA's. The protocols that are mentioned earlier are explained in detail below.

### 2.2.1. DNA Isolation

250 µl Tissue Lysis Buffer (10% 1M Tris pH 7.6, 2.5% 0.2M EDTA, 20% SDS, 4% 5M NaCl) and 6 µl Proteinase K (25 µg/µl, Sigma-Aldrich) is transferred to the Eppendorf tubes that contain 2 mm length clipped tails of the mice. Samples are placed in an orbital shaker incubator for overnight incubation where the temperature and rotational speed are set to 55°C and 75 RPM, respectively. After overnight incubation, samples are centrifuged at 13000 RPM for 10 minutes at RT. The supernatants are transferred into fresh Eppendorf tubes and 250 µl 2-propanol is added to each tube. Then, each tube is gently shaken until DNA precipitate is visible to the naked eye. With a help of a pipette tip, the DNA precipitates are transferred to their new Eppendorf tubes, where the new tubes contain 250 µl 70% ethanol. After that, samples are centrifuged for 1 minute at the max speed of the centrifuge at RT (e.g., 15000 RPM), then supernatant is discarded. The remaining pellets are air-dried at the orbital shaker incubator for 15-20 minutes at 55°C and 75 RPM. Then, 100 µl $dH_2O$ is transferred to the samples, and samples are placed back in the orbital shaker incubator for 1 hour at 55°C and 75 RPM. Samples are stored at -20°C fridges until use.

### 2.2.2. Polymerase Chain Reaction (PCR)

The genotypes of the mice used in this study are determined by PCR. The sequences of primers that are used for genotyping are indicated in Table 2.2.

Extracted DNAs from tails of WT and mutant Neu1 alleles are genotyped by adding 100 ng extracted DNA, 0.4 µM MNTG-1 (Forward Primer), 0.4 µM MNTG-2 (Forward Primer), 0.4 µM LacZ (Reverse Primer), 0.4 mM dNTPs, 1.25 units of Taq

Polymerase, 10X Reaction Buffer and 2 mM $MgCl_2$ in a reaction mixture comprising of 50 µl. The PCR condition for the WT and mutant Neu1 alleles was: 1 cycle x 3 min at 94℃; 30 cycles x 30 sec at 94℃; 30 cycles x 30 sec at 58.1℃; 1 cycle x 2 min at 72℃; and 1 cycle x 10 min at 72℃.

Extracted DNAs from tails of WT and mutant Neu3 alleles are genotyped by adding 100 ng extracted DNA, 0.4 µM Neu3 (Forward Primer), 0.4 µM 552 (Reverse Primer), 0.4 µM 553 (Reverse Primer), 0.4 mM dNTPs, 2.5 units of Taq Polymerase, 10X Reaction Buffer and 3 mM $MgCl_2$ in a reaction mixture comprising of 50 µl. The PCR condition for the WT and mutant Neu3 alleles was: 1 cycle x 3 min at 94℃; 30 cycles x 45 sec at 94℃; 30 cycles x 30 sec at 56℃; 1 cycle x 3 min at 72℃; and 1 cycle x 10 min at 72℃.

Table 2. 2 Primer sequences for genotyping

| Gene | Primer | Primer Sequence |
|---|---|---|
| **Neu1** | MNTG-1 Forward | 5'-GACAGGGATCGCCGGGAGCTATGG-3' |
| | MNTG-2 Forward | 5'-CACCAGGCTGAAGTCATCCTCTGC-3' |
| | LacZ Reverse | 5'-GATAGGTTACGTTGGTGTAGATGGGCG-3' |
| **Neu3** | Neu3 Forward | 5'-AAGCAGAGAACATTCTTGAGAGAGCACAGC-3' |
| | 552 Reverse | 5'-TCGTGCTTTACGGTATCGCCGCTCCCGATT-3' |
| | 553 Reverse | 5'-GTGAGTTCAAGAGCCATGTTGCTGATGGTG-3' |

## 2.3. Mouse Tissue Procedures

Soft and fixed brain tissues of the mice involved in this study are isolated by certain procedures. The detailed methods for those procedures are explained in this section.

### 2.3.1. Dissection of the Mouse Brain

For gene expression and lipid analyses, soft brain tissues of 3-4 weeks old *WT*, *Neu1*$^{-/-}$, *Neu3*$^{-/-}$, and *Neu1*$^{-/-}$ *Neu3*$^{-/-}$ mice are collected and dissected. Mice were initially sacrificed by $CO_2$ and then death is confirmed by cervical dislocation. A small cut is made by a scissor at the base of the mouse skull and excess skin is removed. Muscle tissues are removed from the base of the skull and a small cut along the line of sagittal suture is made with a scissor. Then, the parietal and frontal bones of the skull are removed by pointed dissecting forceps. After that, the mouse brain is collected and placed on ice for dissection. First, the brain is dissected into left and right hemispheres, and then the left and right cortex, cerebellum, thalamus, and hippocampus are collected with the help of a dissecting spatula. After dissection, samples are treated with liquid nitrogen, transported, and stored in a -80℃ freezer immediately. The anatomy of the mouse cortex and cerebellum is depicted in Figures 2.1 and 2.2.

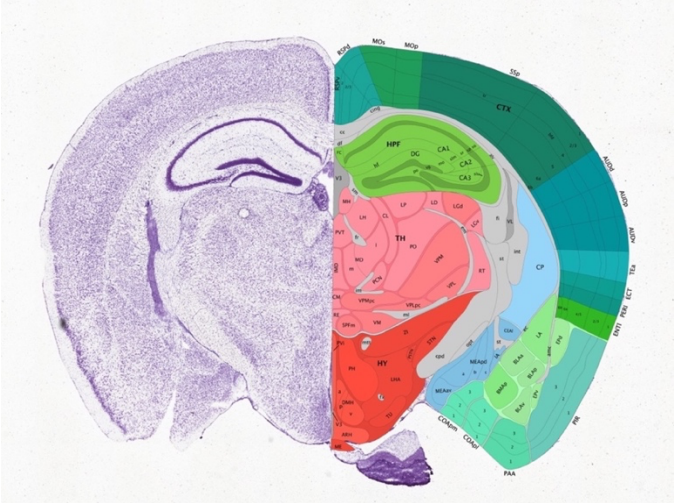


Figure 2. 1. Coronal section and anatomical annotations of mouse cortex from the Allen Mouse Brain Atlas. The cortex region is highlighted in dark green and hippocampal CA1, CA2, and CA3 regions are highlighted in light green.

Source: (2014; Oh et al. 2014; Harris et al. 2019; Lein et al. 2007), mouse.brain-map.org and atlas.brain-map.org

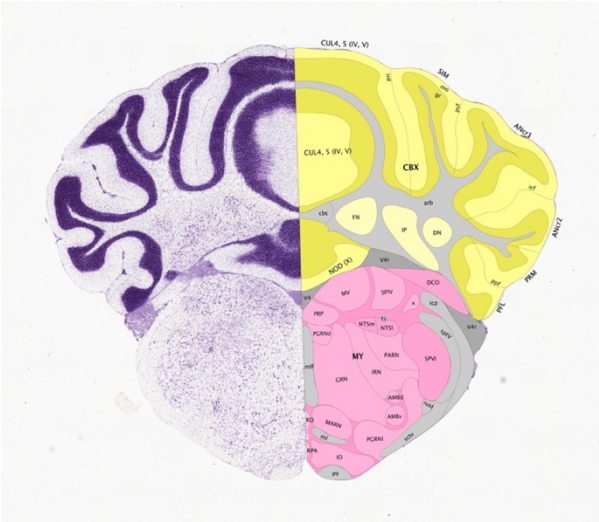


Figure 2. 2. Coronal section and anatomical annotations of mouse cerebellum from the Allen Mouse Brain Atlas. The fiber tracts are highlighted in gray, and the cerebellar cortex is highlighted in shades of yellow. The cerebellar nuclei fastigial nucleus (FN), interposed nucleus (IP), and dentate nucleus (DN) were annotated.

(Source: (2014; Oh et al. 2014; Harris et al. 2019; Lein et al. 2007), mouse.brain-map.org and atlas.brain-map.org)

### 2.3.2. Mouse Transcardial Perfusion and Fixation of the Brain

For immunohistochemical and histochemical analyses, 10 μm sections from fixed brain tissues of 3-4 weeks old *WT*, *Neu1*$^{-/-}$, *Neu3*$^{-/-}$, and *Neu1*$^{-/-}$ *Neu3*$^{-/-}$ mice are used. 4% Paraformaldehyde (PFA, dissolved in 1X PBS) and 0.9% NaCl (physiological saline solution) are prepared to perform the fixation protocol. The mouse to be fixated is anesthetized by intraperitoneal injection with a ketamine and xylazine mixture which is calculated in proportion to its weight. Then, the mouse was placed and stabilized on the perfusion stage to enable easy access to the peritoneal cavity. After that, a small incision to the abdomen of the mouse was done with scissors. Then, the peritoneum was grabbed with blunt forceps and cut to reveal the chest wall. The diaphragm of the mouse was removed carefully to expose the heart. The rib cage was cut carefully in a line that is parallel with the lungs. Then, the heart was incised at the right atrium to decrease the blood flow pressure. Approximately 10-15 ml of physiological saline solution was perfused through the mice at the left ventricle to exsanguinate the mouse. After that, 10

ml of 4% PFA was perfused to fixate the mouse. Then, the brain was collected by removing the parietal and frontal bones carefully. After transcardial perfusion, the collected brain was incubated in 4% PFA for 24 hours. When fixation was completed, the brain was treated with increasing concentrations of sucrose dissolved in 1X PBS to cryopreserve the tissue. The brain was incubated at 10%, sucrose for 2 hours at 4℃, 20% sucrose for 2 hours at 4℃, and 30% sucrose for 24 hours at 4℃, gradually. Finally, the brain was embedded in a tissue cassette containing Optimal Cutting Temperature (OCT) compound where this embedding procedure was done in a dry ice box (-80℃). Frozen samples stored at -80℃ freezer until tissue sectioning.

### 2.3.3. Tissue Sectioning

10 µm sections from fixed and frozen brain tissues were cut coronally by using a cryostat (Leica CM1850 UV, Germany). Tissue sections are transferred to poly-L-lysine coated slides at -20℃ and then immediately stored at -80℃ freezer.

## 2.4. Total RNA Isolation

Cortices and cerebella of 3–4 weeks old *WT*, *Neu1*$^{-/-}$, *Neu3*$^{-/-}$, and *Neu1*$^{-/-}$ *Neu3*$^{-/-}$ mice are used for total RNA isolation. Firstly, the samples were homogenized with tissue grinding beads by using a ball mill homogenizer (Retsch MM 400, Germany). During homogenization, 750 µl and 500 µl Riboex (Geneall, Korea) were used for RNA isolation of the cortex and cerebellum, respectively. After tissues were homogenized, they were incubated at RT for 5 mins. Then, they were centrifuged at 12000 x g for 10 mins at 4℃. Per 1 ml of Riboex that was used, 200 µl chloroform was transferred to the supernatants of the samples after centrifugation. Then, samples were shaken gently and incubated at RT for 2 mins. After that, the samples are centrifuged at 12000 x g for 15 mins at 4℃. Centrifugation results in the phase separation of RNA, DNA, and proteins, respectively. Therefore, the transparent fluid at the upper side of the Eppendorf tube contains total RNA. The upper phase was collected, and then 500 µl 2-propanol was added per 1 ml of Riboex. The samples were gently inverted a few times and then incubated at RT for 10 mins. After incubation, the samples were centrifuged at 12000 x g for 10 mins at 4℃, and subsequently, 2-propanol was removed. Then, 1 ml of 75% ethanol was added per 1 ml

of Riboex to wash RNA samples. After that, the samples are centrifuged at 7500 x g for 5 mins at 4℃. Then, 75% ethanol was removed, and the samples were air-dried for 15 mins. 50 µl RNAse-free water was added to the samples and then, they were placed in a 55℃ water bath for 15 mins to dissolve. The concentrations of the samples were measured by nanodrop spectrometer (NanoPhotometer N50, Implen, Germany).

## 2.5. cDNA Synthesis

The extracted RNAs were converted into cDNAs by using EvoScript Universal cDNA Master Kit (Roche, Switzerland). 10 µl reaction mixture comprising 2 µl reaction buffer, 1 µl enzyme mixture, and 7 µl mixture of 1250 ng/µl RNAs and RNAse-free water were used to generate 125 ng/µl cDNAs. Thermal cycler conditions for the cDNA synthesis were 15 minutes at 42℃; 5 minutes at 85℃; 15 minutes at 65℃. After the reaction was complete, the concentration of the cDNAs was diluted to 50 ng/µl with RNAse-free water.

## 2.6. Real-Time Polymerase Chain Reaction (RT-PCR)

The relative mRNA expression analyses were performed on cDNAs of 3–4 weeks old *WT*, *Neu1*$^{-/-}$, *Neu3*$^{-/-}$, and *Neu1*$^{-/-}$ *Neu3*$^{-/-}$ mice. The internal control gene was selected as the glyceraldehyde-3-phosphate dehydrogenase (GAPDH) gene. The sequences of the primers that are used for gene expression analyses are stated in Table 2.3.

LightCycler® 480 SYBR Green I Master Mix Kit (Roche, Switzerland) was used for performing RT-PCR experiments. The relative gene expression levels were determined in a 20 µl reaction mixture comprising 50 ng/µl cDNAs, 0.4 µM primers, and 10 µl 1X Roche LightCycler 480 SYBR Green I Master Mix. The PCR conditions were 1 cycle x 10 minutes at 95°C; 45 cycles x 20 seconds at 95°C, 15 seconds at 57°C, and 22 seconds at 72°C.

Table 2. 3 The primers that are used in RT-PCR gene expression analyses

| Gene | Primer | Primer Sequence |
|---|---|---|
| **GFAP** | Gfap-F | 5'-AGTTAACATGCAAGAGACAGAG- 3' |
| | Gfap-R | 5'-TAGTCGTTAGCTTTCGTGCTTG- 3' |
| **CCL2** | CCL2-F | 5'-ATGCAGTTAATGCCCCACTC- 3' |
| | CCL2-R | 5'-TTCCTTATTGGGGTCAGCAC- 3' |
| **CCL3** | MIP-1a-F | 5'-TCTGTACCATGACACTCTGC- 3' |
| | MIP-1a-R | 5'-AATTGGCGTGGAATCTTCCG- 3' |
| **CCL5** | RANTES-F | 5'-AGTGCTCCAATCTTGCAGTC- 3' |
| | RANTES-R | 5'-AGCTCATCTCCAAATAGTTT- 3' |
| **MAG** | Mag-F | 5'-TACAACCAGTACACCTTCTCGG- 3' |
| | Mag-R | 5'-ATACAACTGACCTCCACTTCCG- 3' |
| **GAPDH** | GAPDH F | 5'-CCCCTTCATTGACCTCAACTAC- 3' |
| | GAPDH R | 5'-ATGCATTGCTGACAATCTTGAG- 3' |

## 2.7. Immunohistochemistry Analyses

PFA-fixed cortices and cerebella of 3–4 weeks old *WT*, *Neu1*$^{-/-}$, *Neu3*$^{-/-}$, and *Neu1*$^{-/-}$ *Neu3*$^{-/-}$ mice are used for immunohistochemistry analyses. The 10 µm coronal brain sections were mounted on poly-L-lysine coated microscope slides. The images obtained from these immunochemistry analyses were taken by a DP73 camera (DP73, Olympus Corporation, Germany) which is connected to a light microscope (Bx53, Olympus Corporation, Germany).

### 2.7.1. anti-GFAP Staining

The samples were placed in a humidity chamber consisting of a petri dish covered with wet tissue and incubated for 20 minutes on ice and 3-4 minutes at the orbital shaker incubator at 55 °C to allow the samples to reach RT. Then, the samples were placed in a staining dish containing 1X PBS and washed 3 times for 5 minutes. After that,

samples were incubated for 1 hour at a blocking buffer consisting of 10% goat serum and 0.2% Tritonx-100 dissolved in 1X PBS. Then, the samples were incubated overnight at primary antibody GFAP (1:200) at 4°C. The following day, the samples were washed 3 times with 1X PBS for 5 minutes. After that, the samples were incubated for 1 hour at secondary antibody goat anti-rabbit Alexa Fluor 568 (1:500, Abcam, USA) at RT. Then, the samples were washed 3 times with 1X PBS for 5 minutes. Finally, Fluoroshield mounting medium with DAPI (Abcam, USA) was used for mounting the slides.

### 2.7.2. anti-MBP Staining

The samples were placed in a humidity chamber consisting of a petri dish covered with wet tissue and incubated for 20 minutes on ice and 3-4 minutes at the orbital shaker incubator at 55 °C to allow the samples to reach RT. Then, the samples were placed in a staining dish containing 1X PBS and washed for 15 minutes. After that, samples were incubated for 1 hour at a blocking buffer consisting of 10% goat serum, 0.3% Tritonx-100, 2.3% glycine, and 4% BSA dissolved in 1X PBS. Then, the samples were incubated overnight at primary antibody MBP (1:50) at 4°C. The following day, the samples were washed 3 times with 1X PBS for 5 minutes. After that, the samples were incubated for 1 hour at secondary antibody goat anti-rabbit Alexa Fluor 488 (1:500, Abcam, USA) at RT. Then, the samples were washed 3 times with 1X PBS for 5 minutes. Finally, Fluoroshield mounting medium with DAPI (Abcam, USA) was used for mounting the slides.

### 2.7.3. anti-NeuN Staining

The samples were placed in a humidity chamber consisting of a petri dish covered with wet tissue and incubated for 20 minutes on ice and 3-4 minutes at the orbital shaker incubator at 55 °C to allow the samples to reach RT. Then, the samples were placed in a staining dish containing 1X PBS and washed for 10 minutes. The samples were incubated in ice-cold acetone for 15 minutes and washed with 1X PBS 2 times for 5 minutes each. After that, samples were incubated for 1 hour at a blocking buffer consisting of 10% goat serum, 0.3% Tritonx-100, 2.3% glycine, and 4% BSA dissolved in 1X PBS. Then, the samples were incubated overnight at primary antibody NeuN (1:50) at 4°C. The following day, the samples were washed 3 times with 1X PBS for 5 minutes.

After that, the samples were incubated for 1 hour at secondary antibody goat anti-rabbit Alexa Fluor 568 (1:500, Abcam, USA) at RT. Then, the samples were washed 3 times with 1X PBS for 5 minutes. Finally, Fluoroshield mounting medium with DAPI (Abcam, USA) was used for mounting the slides.

## 2.8. Histological Analysis

PFA-fixed cortices and cerebella were used to investigate morphological characteristics of 3–4 weeks old *WT*, *Neu1*$^{-/-}$, *Neu3*$^{-/-}$, and *Neu1*$^{-/-}$ *Neu3*$^{-/-}$ mice. The images obtained from these histological analyses were taken by a DP73 camera (DP73, Olympus Corporation, Germany) which is connected to a light microscope (Bx53, Olympus Corporation, Germany).

### 2.8.1. Hematoxylin & Eosin Staining

The samples were placed in a humidity chamber consisting of a petri dish covered with wet tissue and incubated for 20 minutes on ice and 3-4 minutes at the orbital shaker incubator at 55 °C to allow the samples to reach RT. The samples were placed in a staining dish and washed with $dH_2O$ for 2 minutes. Then, the samples were incubated with hematoxylin (Merck, Germany) for 3 minutes. Excess hematoxylin on the slides was initially removed by washing the samples for 5 minutes in $dH_2O$, then running tap water for 5 minutes. After that, the samples are treated with 1% HCl in 70% ethanol for 30 seconds to render differentiation. Then, the samples are washed in running tap water for 5 minutes and with $dH_2O$ for 2 minutes, respectively. The slides were counterstained with eosin (Merck, Germany) for 1 minute and dehydrated two times with 95% ethanol and 100% ethanol for 2 minutes each. Finally, the slides were mounted with Cytoseal XYL (Thermo Fisher, USA) and covered with cover-glass.

## 2.9. Glycosphingolipid Analysis

The soft cortex tissues from 3–4 weeks old *WT*, *Neu1*$^{-/-}$, *Neu3*$^{-/-}$, and *Neu1*$^{-/-}$ *Neu3*$^{-/-}$ mice were used for glycosphingolipid analysis. Neutral and acidic

glycosphingolipids were isolated from the samples and then loaded into a silica plate separately to perform thin-layer chromatography. The results were scanned by HP Scanner.

### 2.9.1. Isolation of Glycosphingolipids

50 mg cortex tissues were weighed, placed into borosilicate tubes, and homogenized in 1 ml $dH_2O$ by using Ultra Turrax Homogenizer (IKA, Germany). Then the homogenates were sonicated 3 times for 30 seconds with an ultrasonic homogenizer (Bandelin, Germany). After that, the samples were placed on top of a heater which was set to 55 °C, and water in the samples was evaporated with $N_2$ gas. 3 ml acetone was transferred into tubes, and the samples were gently vortexed. Then, the samples were centrifuged for 5 minutes at 2000 RPM. The supernatants were discarded. The samples were treated with acetone 2 times. After that, 1.5 ml Chloroform: Methanol: Water (10:10:1) was transferred into tubes, and the samples were gently vortexed. Then, the samples were centrifuged for 5 minutes at 2000 RPM. The supernatants were collected in neutral tubes by using glass Pasteur pipettes carefully to not disturb the pellet. The samples were treated with Chloroform: Methanol: Water (10:10:1) 3 times. Subsequently, 3 ml Chloroform: Methanol: Water (30:60:8) was transferred into tubes, and the samples were gently vortexed. Then, the samples were centrifuged for 5 minutes at 2000 RPM. The supernatants were continued to be collected in the same neutral tubes. The samples were treated with Chloroform: Methanol: Water (30:60:8) 3 times. The resulting fluid comprises total glycosphingolipids; neutral and acidic.

### 2.9.2. DEAE Sephadex A-25 Resin and Ion-Exchange Column Preparation

DEAE Sephadex A-25 (A=anionic) is used as the stationary phase of the column chromatography assay. The resin contains positively charged Diethylaminoethyl cellulose residues. Negatively charged acidic glycosphingolipids are trapped in the resin by interacting with positively charged residues where neutral glycosphingolipids flow through. Since gangliosides are negatively charged glycosphingolipids this method of

separation is highly effective to collect neutral glycosphingolipids and gangliosides separately. DEAE Sephadex A-25 (GE Healthcare) that is used for this experiment was in the chloride form. In order to accomplish a successful separation of the neutral glycosphingolipids and gangliosides, it is converted into acetate form.

1 g of DEAE Sephadex A-25 resin was swelled by washing it three times in Chloroform: Methanol: 0.8M sodium acetate (30:60:8) 3 times. After overnight incubation at RT, the resin was washed with Chloroform: Methanol: Water (30:60:8) 3 times and stored at RT until usage.

Glass wool was washed with Chloroform: Methanol: Water (30:60:8). Then, the columns (225 mm Pasteur pipettes) were plugged with glass wool to prevent the resin from flowing through. After that, the columns were washed with Chloroform: Methanol: Water (30:60:8) 3 times and then, one time with Chloroform: Methanol: Water (10:10:1).

### 2.9.3. Separation of Neutral and Acidic Glycosphingolipids

Total glycosphingolipids that were extracted earlier are mobile phase and they were transferred into the columns. After total glycosphingolipids flowed, 4 ml methanol was transferred into the columns. The fluid that was collected contained the neutral glycosphingolipids and they were evaporated with $N_2$ gas at 55 °C immediately after collection.

The acidic glycosphingolipids were trapped in the resin. Therefore, they were collected by disrupting the interaction between the positively charged resin and negatively charged glycosphingolipids. 5.5 ml 0.5M potassium acetate (dissolved in methanol) was transferred into the columns and then the acidic glycosphingolipids were collected in a fresh tube. Since acidic glycosphingolipids that are collected contained potassium salt, they were desalted by Supelclean LC18 SPE 100 mg columns. The Supelclean columns were prepared by washing them with 2 ml methanol and then 2 ml 0.5M potassium acetate. After that, the samples were transferred into the columns and the salt was removed by passing through the column. The acidic glycosphingolipids that are contained within the column were washed with 10 ml $dH_2O$ to remove the remaining salt. Then, acidic glycosphingolipids were collected by transferring 4 ml methanol and after methanol, 4.75 ml Methanol: Chloroform (1:1). Finally, the acidic glycosphingolipids were evaporated by $N_2$ gas at 55 °C.

### 2.9.4. Thin Layer Chromatography (TLC)

TLC tank was washed with $dH_2O$ and Chloroform: Methanol: Water (30:60:8) solution. Then, Chloroform: Methanol: 0.2% $CaCl_2$ (dissolved in $dH_2O$) (60:35:8) solution was prepared as the TLC solvent. After that, the tank was incubated for 2.5 hours to allow the equilibrium of the solution.

As a TLC plate, TLC Silica Gel 60 glass plate 20x20 cm was used. Before usage, the plate was heated at 90 °C for an hour. After the plate was cooled off, the neutral and acidic glycosphingolipid samples were loaded in the plate by using Linomat V (CAMAG, Switzerland). The samples were dissolved in 100 µl Chloroform: Methanol: Water (10:10:1) and loaded into the plate one at a time. 11 cm was chosen as a retention factor, and it is marked on the plate. After that, the plate was placed into the tank carefully without causing any wave-like motion of the solvent. After the solvent reached 11 cm, the plate was removed carefully to be visualized by orcinol staining.

Orcinol was prepared in a diffuser with 11.25 ml $dH_2O$, 3.75 ml $H_2SO_4$, and 0.06g g orcinol, respectively. First, $dH_2O$ and $H_2SO_4$ were mixed and allowed to be cooled off since it is an exothermic reaction. Finally, orcinol was added and then sprayed to the plate from approximately 30 cm distance. The plate was visualized at 120 °C by a TLC heater (CAMAG, Switzerland). Finally, when the bands were visible, it is removed from the heater and scanned by HP Scanner.

## 2.10. Statistical Analyses

The statistical analyses were performed by utilizing Graphpad Prism 7 Software (Graphpad Software, USA). One-way ANOVA test was used for the analyses of RT-PCR and immunohistochemistry experiments. Standard Error of Mean (SEM) was used to calculate the variability of the data and statistical significance was demonstrated as a p-value of less than 0.05.

# CHAPTER 3

# RESULTS

## 3.1. Genotyping of Mice

By using Neu1 and Neu3 specific primers (Table 2.2), the genotypes of *WT*, *Neu1*$^{-/-}$, *Neu3*$^{-/-}$, and *Neu1*$^{-/-}$ *Neu3*$^{-/-}$ mice were confirmed (Figure 3.1).

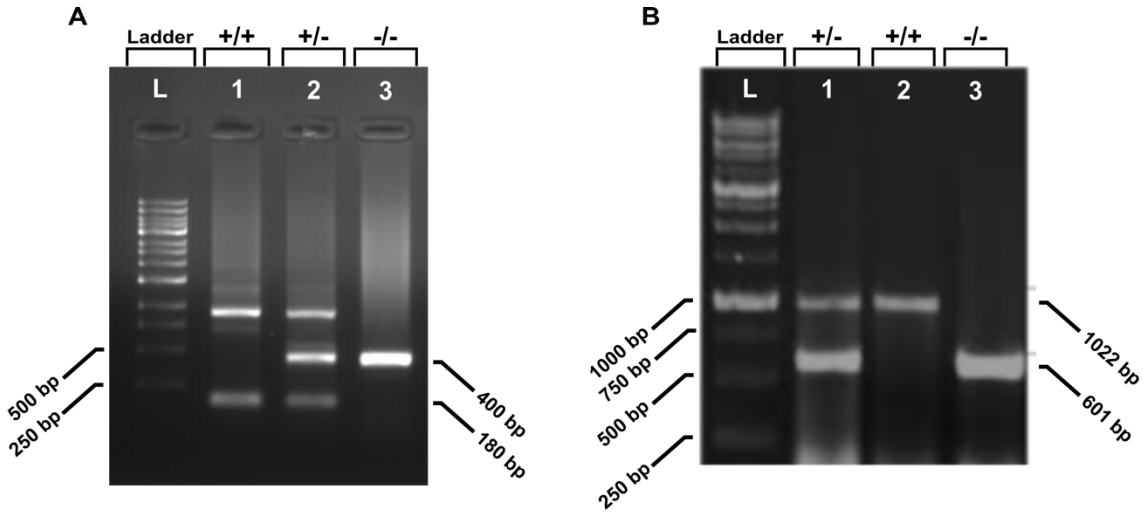


Figure 3. 1. Neu1 and Neu3 PCR Products

The genotype of the homozygous Neu1 allele was confirmed by a DNA fragment of 180 bp, and the nullizygous Neu1 allele was confirmed by a DNA fragment of 400 bp.

The genotype of the homozygous Neu3 allele was confirmed by a DNA fragment of 1022 bp, and the nullizygous Neu3 allele was confirmed by a DNA fragment of 601 bp.

## 3.2. Morphological Abnormalities in *Neu1*$^{-/-}$ *Neu3*$^{-/-}$ Mice Compared to Its Littermates

*Neu1*$^{-/-}$ *Neu3*$^{-/-}$ mice were generated by the inbred crossing of *Neu1*$^{+/-}$ *Neu3*$^{-/-}$ parents (Table 2.1). In the breeding cage, they were distinguished by their smaller appearance, a short lifetime of 2-3 weeks, and tremoring compared to their littermates. Body length measurements revealed that *Neu1*$^{-/-}$ *Neu3*$^{-/-}$ mice were 21.5% shorter than their littermates. Additionally, there was a substantial amount of difference in weight average of the *Neu1*$^{-/-}$ *Neu3*$^{-/-}$ mice. They were 46.9% lighter than their littermates (Figure 3.2).

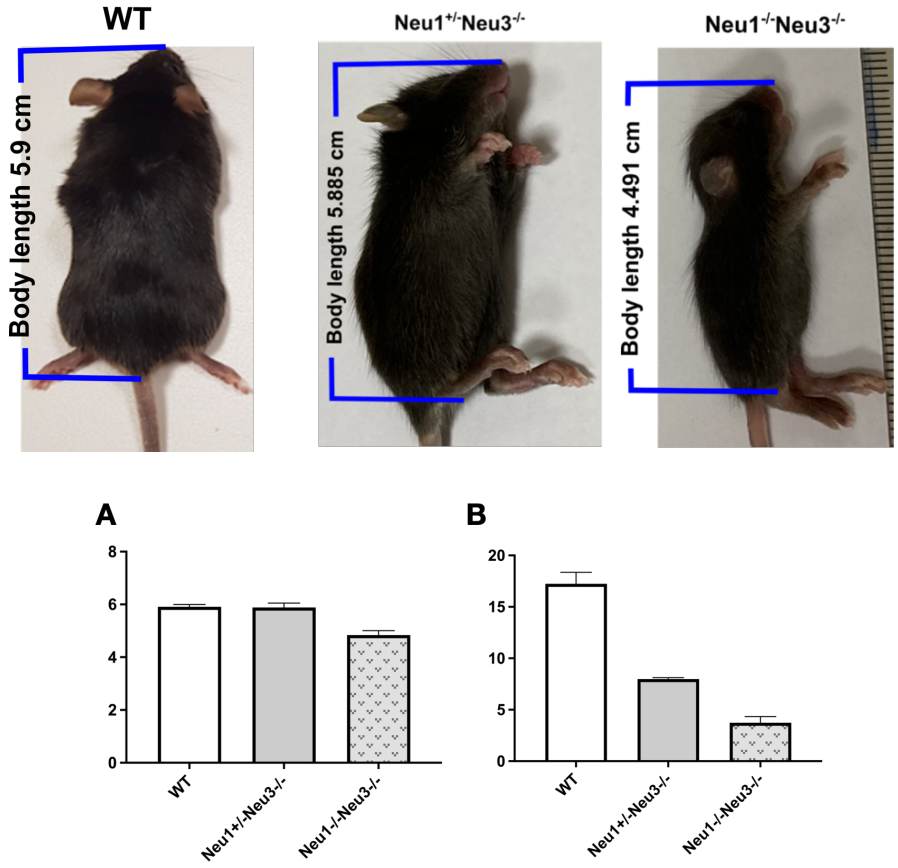


Figure 3. 2. Body length (A) and body weight (B) comparison between WT, Neu1$^{-/-}$, and Neu3$^{-/-}$ mice.

## 3.3. Altered Levels of Cytokines in Combined Deficiency of Neuraminidase 1 and Neuraminidase 3

The expression of neuroinflammatory cytokines is measured in cortices and cerebella of *WT, Neu1*$^{-/-}$*, Neu3*$^{-/-}$*, Neu1*$^{-/-}$ *Neu3*$^{-/-}$ mouse models, and alterations in the expression levels of CCL2 (MCP-1), CCL3 (MIP-1α), and CCL5 (RANTES) are observed.

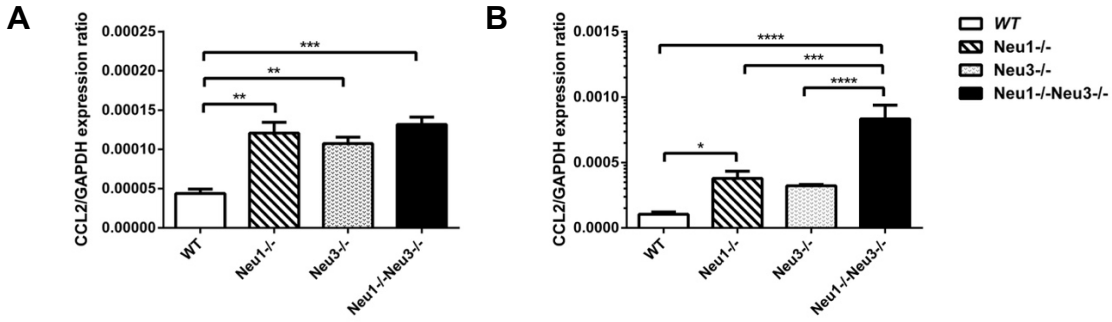


Figure 3. 3. Relative expression levels of inflammatory cytokine CCL2 in the cortex (A) and cerebellum (B) of WT, Neu1-/-, Neu3-/-, Neu1-/- Neu3-/- mouse models. Ages of the mice range from 3-4 weeks. One- way ANOVA was used for statistical analysis (*p < 0.05, **p <0.025, ***p < 0.01, and ****p < 0.001).

Real-time PCR results revealed that in the mouse cortex, there is a significant increase in the CCL2 expression in the *Neu1*$^{-/-}$*, Neu3*$^{-/-}$*, Neu1*$^{-/-}$ *Neu3*$^{-/-}$ mice compared to WT mice as 2.75 (**p <0.025), 2.45 (**p <0.025), and 3-fold (***p < 0.01), respectively (Figure 3.3A). In the cerebellum, there was also a significant 8-fold (****p < 0.001) increase in CCL2 expression of *Neu1*$^{-/-}$ *Neu3*$^{-/-}$ mice compared to WT mice (Figure 3.3B). And compared to *Neu1*$^{-/-}$ and *Neu3*$^{-/-}$ mice, the expression of CCL2 in the cerebellum of *Neu1*$^{-/-}$ *Neu3*$^{-/-}$ mice was higher: 2.2-fold (***p < 0.01) for *Neu1*$^{-/-}$ mice and 2.6-fold (and ****p < 0.001) for *Neu3*$^{-/-}$ mice. Additionally, there was a 3.6-fold (*p < 0.05) increase in CCL2 expression of *Neu1*$^{-/-}$ mice compared to WT mice. Moreover, CCL2 accumulation in the cerebellum of *Neu1*$^{-/-}$ *Neu3*$^{-/-}$ mice is 6.3-fold higher than that in the cortex of *Neu1*$^{-/-}$ *Neu3*$^{-/-}$ mice. For WT, *Neu1*$^{-/-}$, and *Neu3*$^{-/-}$ mice the difference between CCL2 expression in the cerebellum and cortex is 2.3, 3.1, and 3-fold, respectively, where expression in the cerebellum is higher.

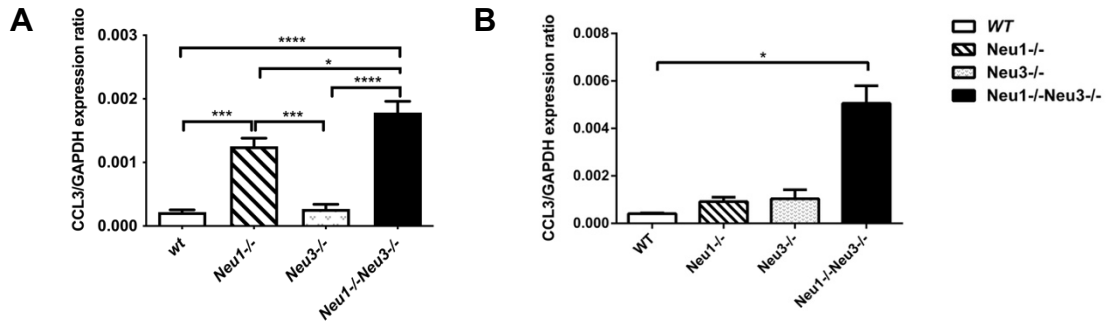


Figure 3. 4. Relative expression levels of inflammatory cytokine CCL3 in the cortex (A) and cerebellum (B) of WT, Neu1-/-, Neu3-/-, Neu1-/- Neu3-/- mouse models. Ages of the mice range from 3-4 weeks. One- way ANOVA was used for statistical analysis (*$p < 0.05$, **$p < 0.025$, ***$p < 0.01$, and ****$p < 0.001$).

There is a substantial increase in the cortical expression of CCL3 when *Neu1*$^{-/-}$, and *Neu1*$^{-/-}$ *Neu3*$^{-/-}$ mice compared with WT mice: 5.73 (***$p < 0.01$), and 8.1-fold (****$p < 0.001$), respectively (Figure 3.4A). However, there is not any distinguishable change observed between WT and *Neu3*$^{-/-}$ mice in the cortex (Figure 3.4A). Additionally, CCL3 expression in the cortex of *Neu1*$^{-/-}$ mice is 4.6-fold (***$p < 0.01$) higher than that of *Neu3*$^{-/-}$ mice.

In the cerebellum, the CCL3 expression was almost the same in WT, *Neu1*$^{-/-}$, and *Neu3*$^{-/-}$ mice (Figure 3.4B). However, when WT mice and *Neu1*$^{-/-}$ *Neu3*$^{-/-}$ mice were compared there was a considerable 12.75-fold (*$p < 0.05$) increase in the CCL3 cerebellar expression of *Neu1*$^{-/-}$ *Neu3*$^{-/-}$ mice. Additionally, CCL3 expression in the cerebellum of *Neu1*$^{-/-}$ *Neu3*$^{-/-}$ mice is 4.65-fold higher than that of in cortex.

A distinct decrease in the CCL5 expression in the cortex is present (Figure 3.5A). Comparison between WT and *Neu1*$^{-/-}$ *Neu3*$^{-/-}$ mice reveals a 4.65-fold (**$p < 0.025$) decrease in the CCL5 expression in the cortex of double knockout mice with respect to WT mice. On the other hand, there is a 2-fold (**$p < 0.025$) increase in the CCL5 expression of the *Neu1*$^{-/-}$ *Neu3*$^{-/-}$ mice compared to WT mice (Figure 3.5B).

CCL5 expression in the cerebellum showed several other intriguing alterations such as a 1.7-fold (*$p < 0.05$) increase in CCL5 expression of *Neu1*$^{-/-}$ mice compared to WT mice and a 2.1 (**$p < 0.025$) and 2.5-fold (**$p < 0.025$) decrease in CCL5 cerebellar expression in *Neu3*$^{-/-}$ mice compared to *Neu1*$^{-/-}$ and *Neu1*$^{-/-}$ *Neu3*$^{-/-}$ mice, respectively

(Figure 3.5B). In addition to that, CCL5 expression in *Neu1*$^{-/-}$ *Neu3*$^{-/-}$ mice was 12-fold higher in the cerebellum with respect to the expression level in the cortex.

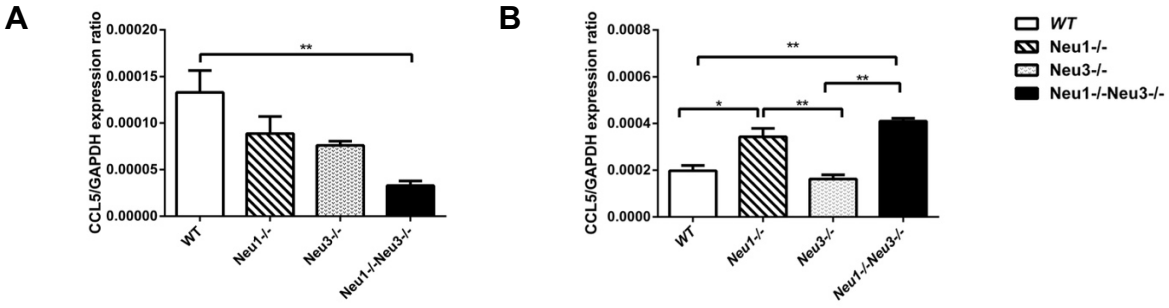


Figure 3. 5. Relative expression levels of inflammatory cytokine CCL5 in the cortex (A) and cerebellum (B) of WT, Neu1-/-, Neu3-/-, Neu1-/- Neu3-/- mouse models. Ages of the mice range from 3-4 weeks. One- way ANOVA was used for statistical analysis (*p < 0.05, **p < 0.025, ***p < 0.01, and ****p < 0.001).

## 3.4. GFAP Expression in The Mouse Cortex and Cerebellum

GFAP expression in the cortex showed a noticeable change. *Neu1*$^{-/-}$ *Neu3*$^{-/-}$ mice expressed GFAP 4-times higher (****p < 0.001) in the cortex when they were compared with WT mice (Figure 3.6A). There was a 1.8-fold (*p < 0.05) decrease in the cortical expression of GFAP in *Neu1*$^{-/-}$ mice compared to WT mice. A comparison of *Neu1*$^{-/-}$ mice, and *Neu3*$^{-/-}$ mice with *Neu1*$^{-/-}$ *Neu3*$^{-/-}$ mice demonstrates that in the mouse cortex, GFAP expression of *Neu1*$^{-/-}$ *Neu3*$^{-/-}$ mice is 7.2 and 2.6-fold higher than that of *Neu1*$^{-/-}$ mice, and *Neu3*$^{-/-}$ mice, respectively (Figure 3.6A).

In the mouse cerebellum, there was a substantial increase in the GFAP expression of *Neu1*$^{-/-}$ *Neu3*$^{-/-}$ mice. GFAP expression was 17-fold higher (***p < 0.01) in *Neu1*$^{-/-}$ *Neu3*$^{-/-}$ mice than that of WT mice. Moreover, there was 11.9 (***p < 0.01) and 6.4-fold (***p < 0.01) increase in GFAP expression of *Neu1*$^{-/-}$ *Neu3*$^{-/-}$ mice compared to *Neu1*$^{-/-}$ and *Neu3*$^{-/-}$ mice. Additionally, there was a 1.6-fold increase in the GFAP expression in the cerebellum in comparison with the cortex.

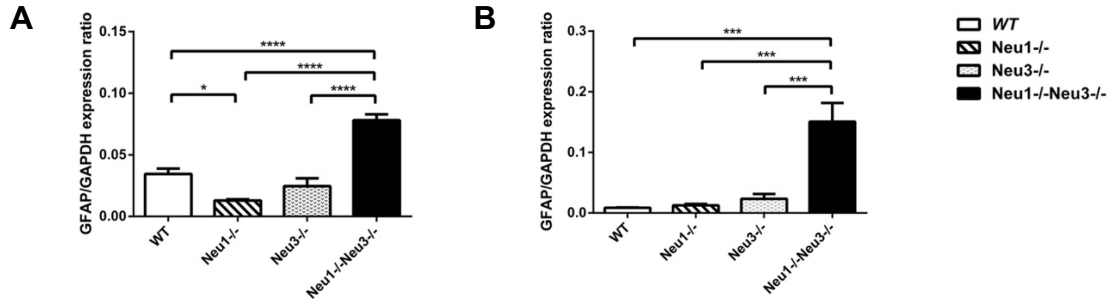


Figure 3. 6. Relative expression levels of glial fibrillary acidic protein (GFAP) in the cortex (A) and cerebellum (B) of WT, Neu1-/-, Neu3-/-, Neu1-/-Neu3-/- mouse models. Ages of the mice range from 3-4 weeks. One-way ANOVA was used for statistical analysis (*p < 0.05, **p < 0.025, ***p < 0.01, and ****p < 0.001).

GFAP immunochemistry staining in several mouse brain sections demonstrates that there is clear evidence of activated astrocyte presence in *Neu1*$^{-/-}$ *Neu3*$^{-/-}$ mice (Figure 3.7 J-O). GFAP intensity in the hippocampal CA3 region was 2.25-fold (*p < 0.05) higher in *Neu1*$^{-/-}$ *Neu3*$^{-/-}$ mice (Figure 3.7J) compared to WT mice (Figure 3.7A). In CA3 regions of *Neu1*$^{-/-}$, and *Neu3*$^{-/-}$ mice, GFAP intensity was similar to WT mice (Figure 3.7D, and G).

The cortex region GFAP staining also showed that there is an increase in the GFAP intensity of *Neu1*$^{-/-}$ *Neu3*$^{-/-}$ mice compared to WT mice by 2.45-fold (*p < 0.05) (Figure 3.7 B, and K). Additionally, there was no correlation between WT, Neu*1*$^{-/-}$ and *Neu3*$^{-/-}$ mice in the cortex GFAP intensity (Figure 3.7B, E, and H), similar to the result in the CA3 section (Figure 3.7A, D, and G).

There was a remarkable increase in GFAP intensity in the cerebellum of *Neu1*$^{-/-}$ *Neu3*$^{-/-}$ mice compared to WT, *Neu1*$^{-/-}$ and *Neu3*$^{-/-}$ mice by 4.6 (****p < 0.001), 4.25 (****p < 0.001), and 2.21-fold (***p < 0.01), respectively (Figure 3.7C,F,I,L). Additionally, stellation of the astrocytes was visible in *Neu1*$^{-/-}$ *Neu3*$^{-/-}$ mice, especially the protrusions of the astrocytes in the white matter (Figure 3.7L) as they were not present in the other cerebellum sections.

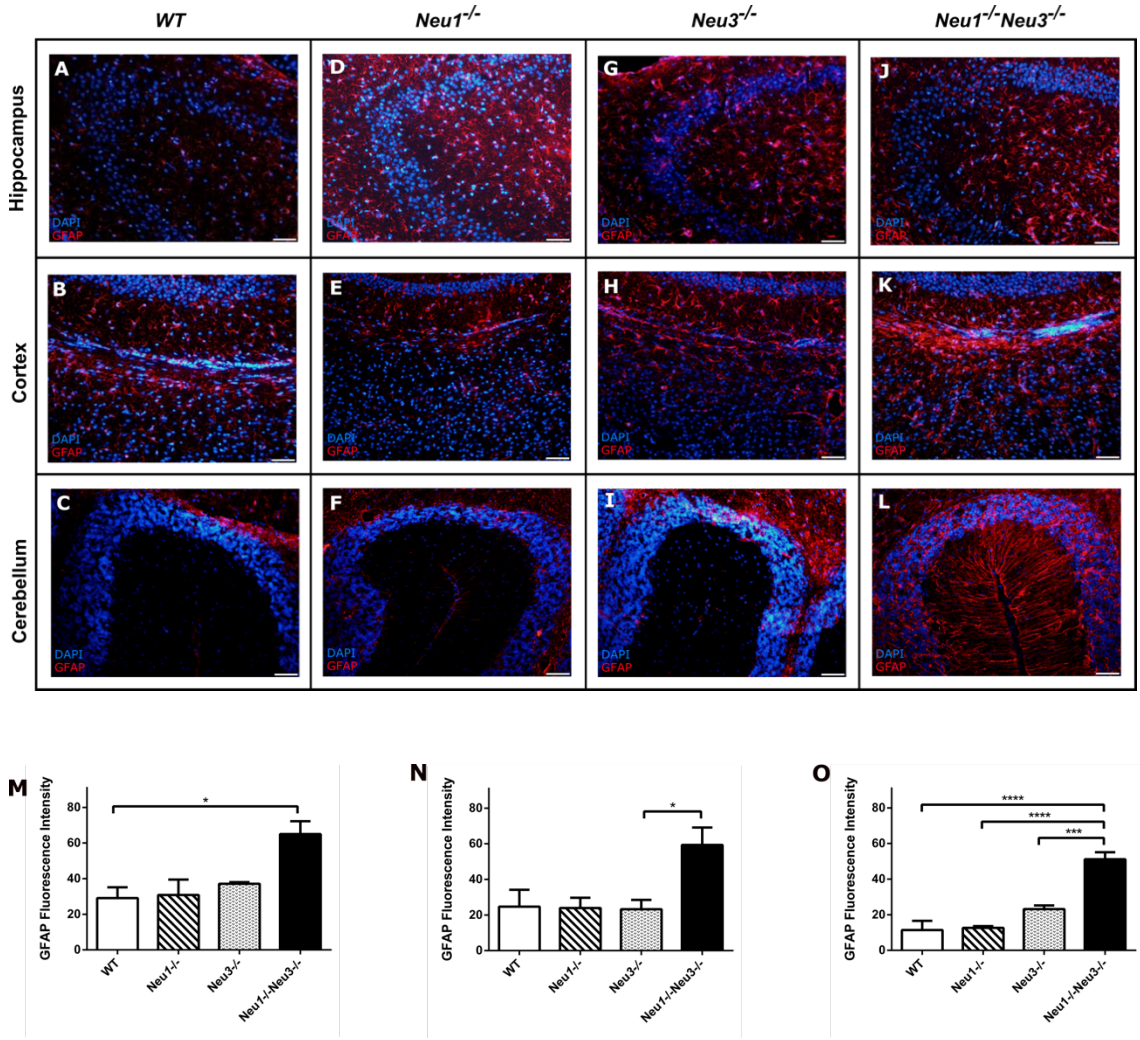


Figure 3. 7. Astrocyte detection in hippocampus, cortex, and cerebellum of WT (A-C), Neu1-/- (D-F), Neu3-/-(G-I), (J-L) Neu1-/- Neu3-/- mouse models presented by GFAP immunohistochemical staining. The histograms represent the quantification of astrocytes in the hippocampus, cortex, and cerebellum (M, N, and O respectively). One- way ANOVA was used for statistical analysis (*p < 0.05, **p < 0.025, ***p < 0.01, and ****p < 0.001). Ages of the mice range from 3-4 weeks. Magnification: 20X (A-L).

## 3.5. MAG Expression in The Mouse Cortex and Cerebellum

There was no correlation found in MAG expression in the cortex (Figure 3.8A) and cerebellum (Figure 3.8B). Additionally, MAG expression was not either decreased or increased when compared between the cortex and cerebellum. The only difference was a slight decrease in the cortex of *Neu1*$^{-/-}$ *Neu3*$^{-/-}$ mice compared to WT mice (Figure 3.8A).

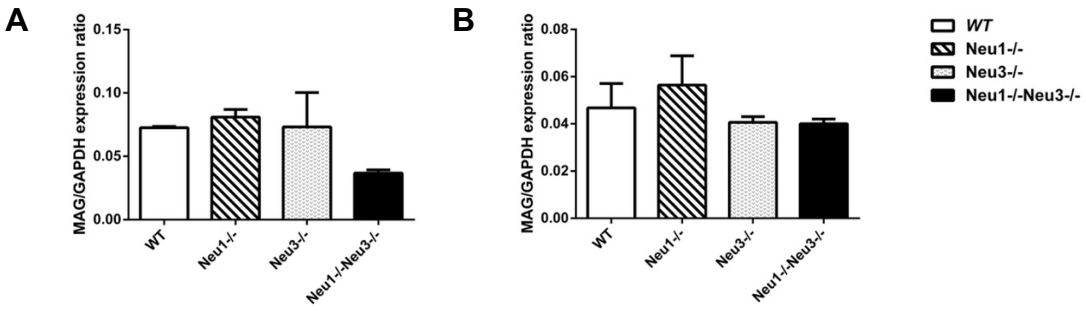


Figure 3. 8. Relative expression levels of myelin-associated glycoprotein (MAG) in the cortex (A) and cerebellum (B) of WT, Neu1-/-, Neu3-/-, Neu1-/- Neu3-/- mouse models. Ages of the mice range from 3-4. One- way ANOVA was used for statistical analysis (*p < 0.05, **p < 0.025, ***p < 0.01, and ****p < 0.001).

MBP immunohistochemical staining in mouse cerebellum region revealed similar results to MAG expression levels. However, in the mouse cortex, there was a significant decrease in MAG intensity of *Neu1*$^{-/-}$ *Neu3*$^{-/-}$ mice (Figure 3.9I) with respect to WT and *Neu3*$^{-/-}$ mice by 2.29-fold (****p < 0.001) and 2.16-fold (***p < 0.01), respectively.

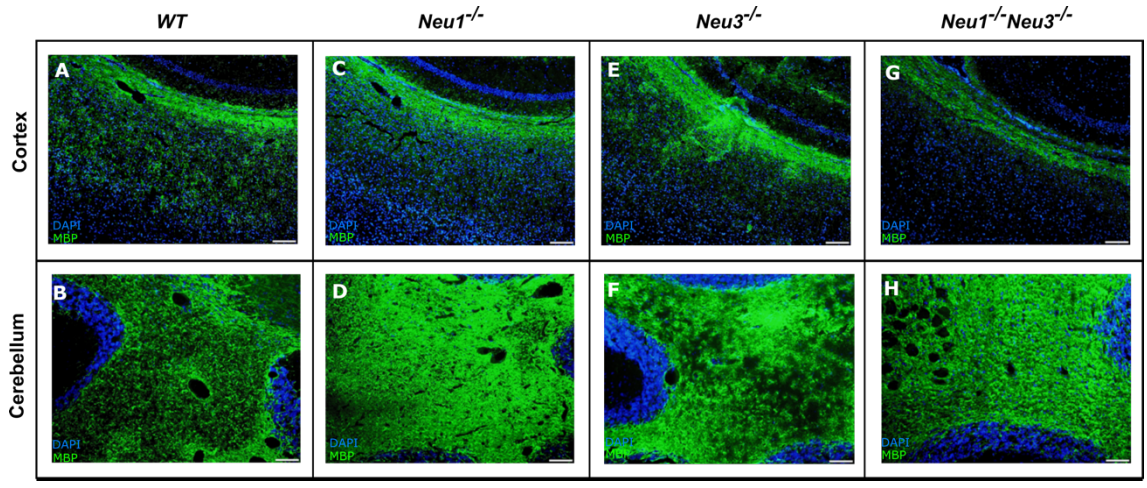


Cont. on next page

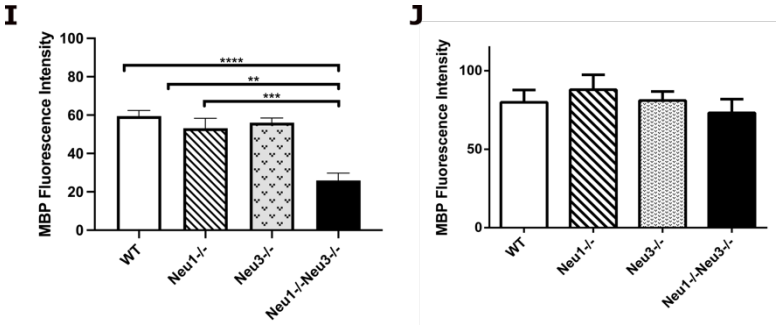


Figure 3. 9. (cont.) Oligodendrocyte detection in cortex and cerebellum of WT (A, B), Neu1-/- (C, D), Neu3-/- (E, F), (G, H) Neu1-/- Neu3-/- mouse models presented by myelin basic protein (MBP) immunohistochemical staining. The histograms represent the quantification of oligodendrocytes in cortex (I) and cerebellum (J). One- way ANOVA was used for statistical analysis (*p < 0.05, **p < 0.025, ***p < 0.01, and ****p < 0.001). Ages of the mice range from 3-4 weeks. Magnification: 20X (A-H).

## 3.6. NeuN Expression in The Mouse Cortex and Cerebellum

Immunohistochemical analyses showed that there was a substantial decrease in the NeuN expression in several sections of the mouse brain (Figure 3.10). In the mouse cortex (Figure 3.10A,D,G,J), when compared to WT, *Neu1*$^{-/-}$ and *Neu3*$^{-/-}$ mice, the intensity of NeuN was decreased in *Neu1*$^{-/-}$ *Neu3*$^{-/-}$ mice by 4.59-fold (*p < 0.05), 3.77-fold (**p < 0.025), and 3.77-fold (*p < 0.05). In the thalamus (Figure 3.10N), a significant decrease in NeuN intensity was observed in *Neu1*$^{-/-}$ *Neu3*$^{-/-}$ mice when compared to WT, *Neu1*$^{-/-}$ and *Neu3*$^{-/-}$ mice by 3.9-fold (**p < 0.025), 5.7-fold (***p < 0.01), and 6.46-fold (****p < 0.001), respectively. There was also a significant increase observed in *Neu3*$^{-/-}$ mice compared to WT mice as 1.65-fold (**p < 0.025).

A substantial decrease in NeuN intensity was observed in the mouse cerebellum (Figure 3.10 C,F,I,L). When compared to WT, and *Neu3*$^{-/-}$ mice, there was a significant decrease in NeuN expression in *Neu1*$^{-/-}$ *Neu3*$^{-/-}$ mice (Figure 3.10 O) by 2.3-fold (*p < 0.05) and 1.7-fold (**p < 0.025).

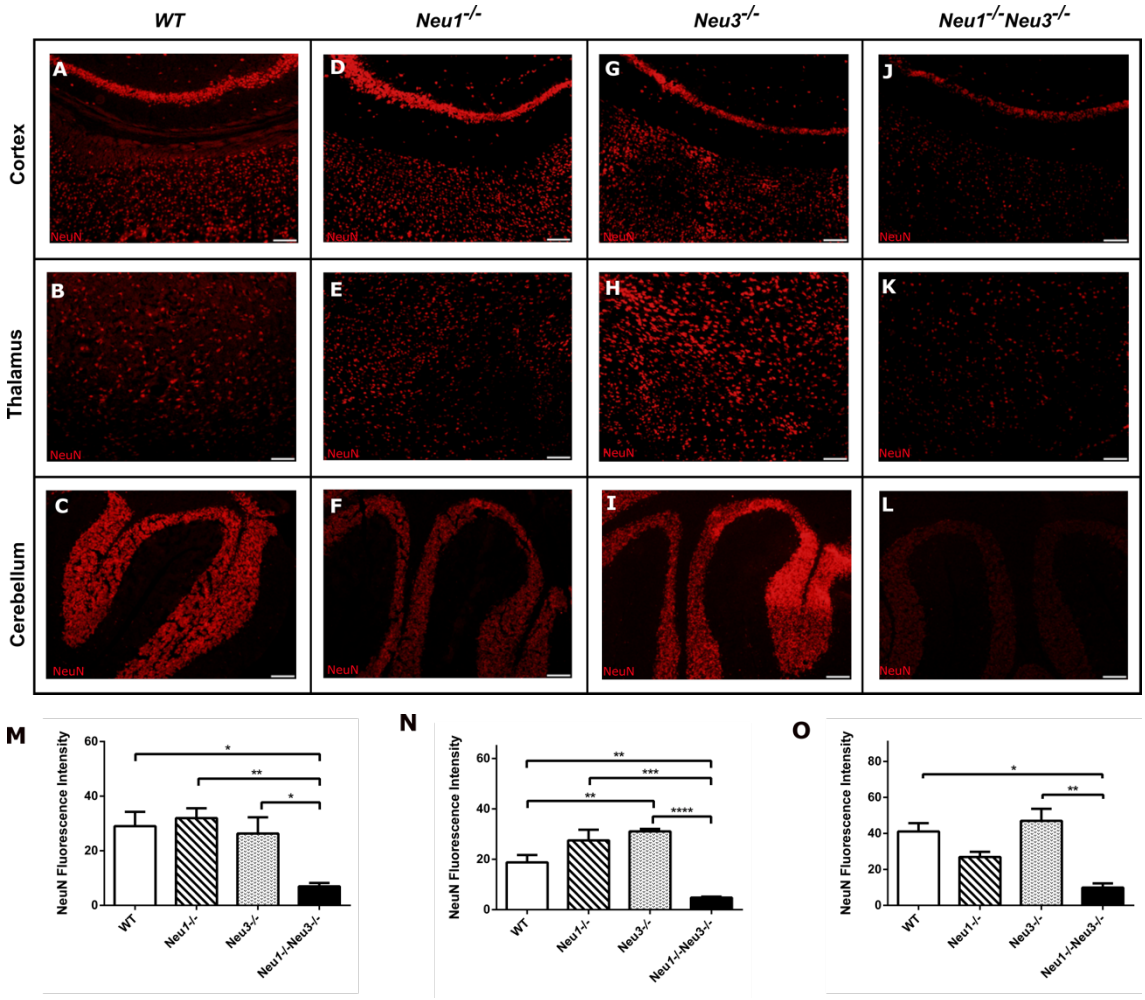


Figure 3. 10. Neuronal density detection in hippocampus, cortex, and cerebellum of WT (A-C), Neu1-/- (D-F), Neu3-/-(G-I), (J-L) Neu1-/- Neu3-/- mouse models presented by neuronal nuclear protein (NeuN) immunohistochemical staining. The histograms represent the quantification of neuronal density in cortex (M), thalamus (N) and cerebellum (O). One- way ANOVA was used for statistical analysis (*p < 0.05, **p < 0.025, ***p < 0.01, and ****p < 0.001). Ages of the mice range from 3-4 weeks. Magnification: 10X (cortex and thalamus), and 20X (cerebellum).

## 3.7. Morphologic Characteristics of Neuraminidase 1 and Neuraminidase 3 Combined Deficiency

Morphological staining in the mouse cortex region revealed the presence of lysosomal vacuolization in *Neu1*$^{-/-}$ *Neu3*$^{-/-}$ mice (Figure 3.11 G-H). There was not any decrease in the hippocampal CA3 region pyramidal neurons observed. In the cortex of *Neu1*$^{-/-}$ and *Neu3*$^{-/-}$ mice there was not any lysosomal vacuolization observed.

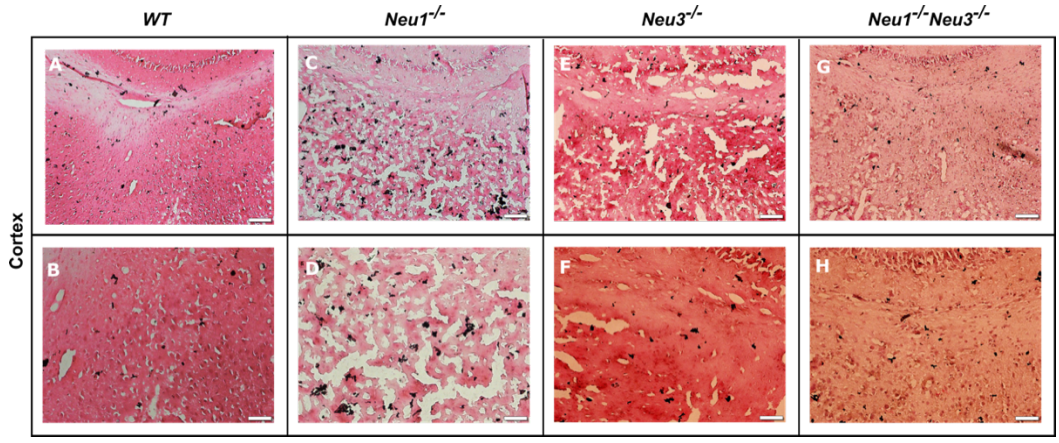


Figure 3. 11. Brain histopathological phenotype of WT (A, B), Neu1-/- (C, D), Neu3-/- (E,F), (G,H) Neu1-/- Neu3-/- mouse models presented by Hematoxylin & Eosin staining of mouse cortex regions. Ages of the mice range from 3-4 weeks. Magnification: A, C, E, G; 10X and B, D, F, H; 20X.

In the cerebellum, there was a disruption in the Purkinje cell layer (PCL) in *Neu1*$^{-/-}$ mice and *Neu1*$^{-/-}$ *Neu3*$^{-/-}$ mice (Figure 3.12 C,D,G,H). There was not any thinning of the granular layer observed in any brain sections of the mice. Additionally, in *Neu1*$^{-/-}$ *Neu3*$^{-/-}$ mice there was lysosomal vacuolization present in the molecular layer of cerebellum (Figure 3.12 G).

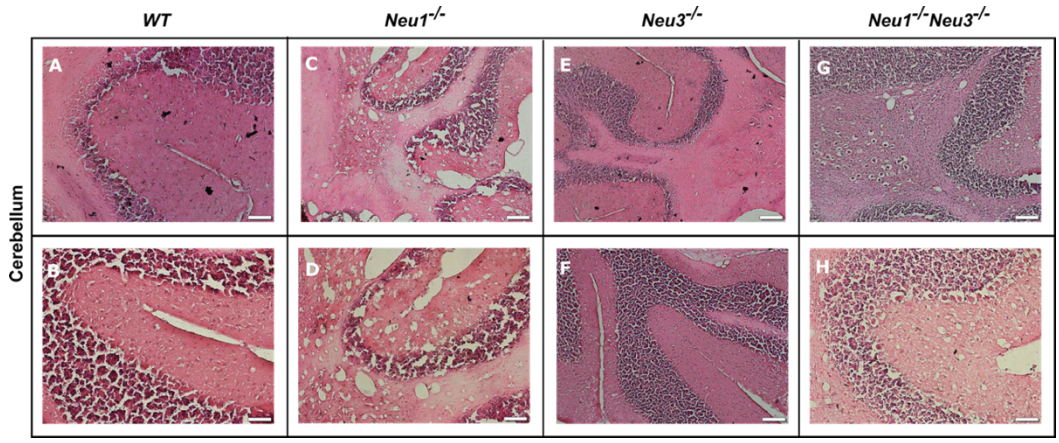


Figure 3. 12. Brain histopathological phenotype of WT (A, B), Neu1-/- (C, D), Neu3-/- (E, F), (G, H) Neu1-/- Neu3-/- mouse models presented by Hematoxylin & Eosin staining of mouse cerebellum regions. Ages of the mice range from 3-4 weeks. Magnification: A, C, E, G; 10X and B, D, F, H; 20X.

## 3.8. Altered Ganglioside Expression in *Neu1*$^{-/-}$ *Neu3*$^{-/-}$ Mouse Cortex

Thin-layer chromatography results demonstrated that there was a significant decrease in ganglioside precursors lactosylceramide (LacCer) and galactosylceramide (GalCer) levels in the cortex of *Neu1*$^{-/-}$ *Neu3*$^{-/-}$ mice (Figure 3.13). Additionally, *Neu1*$^{-/-}$ mice also showed a decrease in the GalCer level. Moreover, ganglioside expression of *Neu1*$^{-/-}$ *Neu3*$^{-/-}$ mice was significantly altered compared to WT mice as GD3 expression was present (Figure 3.13).

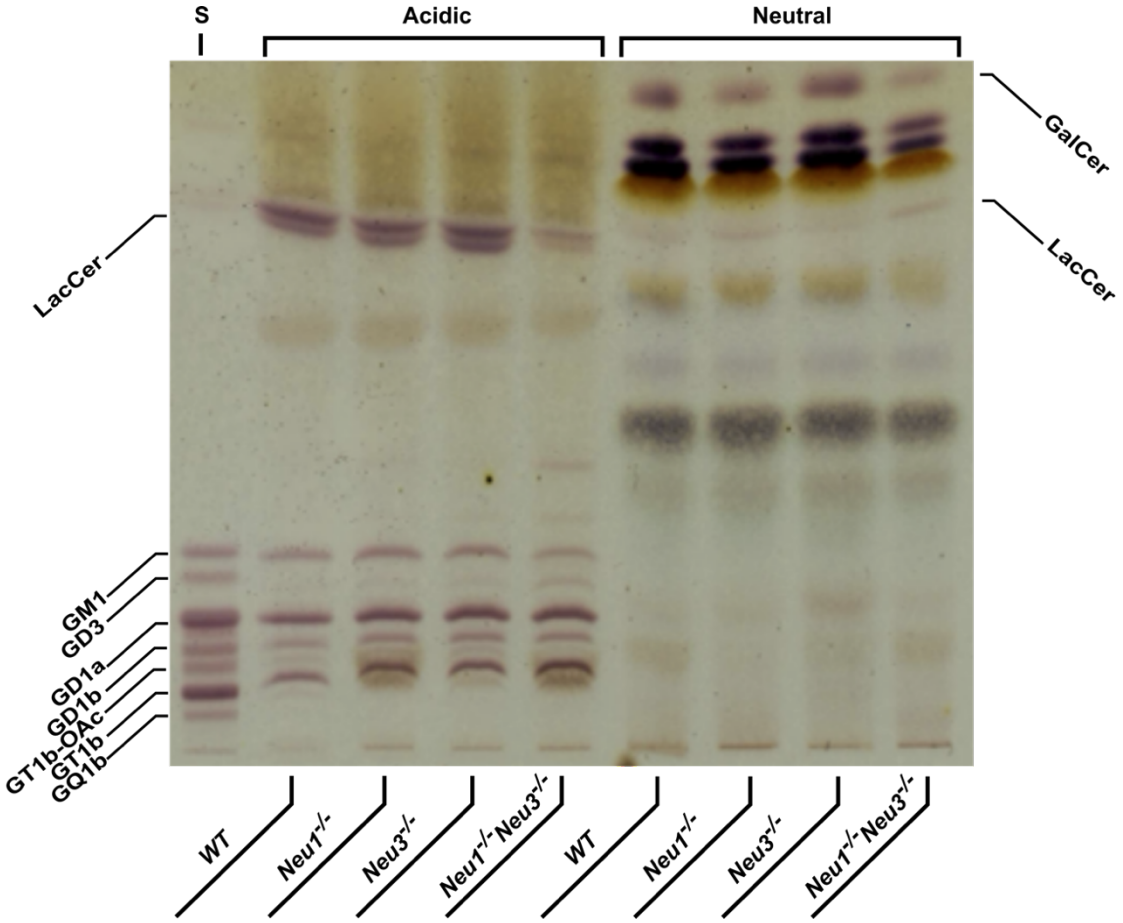


Figure 3. 13. Thin-layer chromatography results of acidic and neutral glycosphingolipids from the cortex of WT, Neu1-/-, Neu3-/-, Neu1-/-Neu3-/- mice. Ages of mice range from 3-4 weeks. 70 µl acidic gangliosides and 25 µl neutral gangliosides were loaded in the silica plate.

# CHAPTER 4

# DISCUSSION

Pathology in the central nervous system (CNS) is present in almost all lysosomal storage diseases (LSD). Excess storage of glycoconjugates in the lysosome is the hallmark of LSDs. Non-dividing neurons are a member of cells of the CNS. Vacuolation in the lysosomes of neurons contributes to the CNS pathophysiology of LSDs. Since neurons are at the post-mitotic phase and not capable of dividing, vacuolation leads to detrimental and irreversible outcomes in CNS. Lysosomes that are structurally impaired due to excess storage could release their contents into the cytoplasm and induce programmed cell death or activate the innate immune system. Continuous stimulation of the immune system leads to chronic inflammation. Inflammation in the central and peripheral nervous system is known as neuroinflammation. Chronic neuroinflammation results in neurodegeneration and eventually, neuronal death.

Non-neuronal members of the CNS are glial cells which comprise astrocytes, oligodendrocytes, and microglia. Microglia are derived from monocytes; they are macrophages of the brain. Monocytes travel from bone marrow to CNS during the late embryonic stage and become resident cells (McGeer and McGeer 1995). Some of the functions of glial cells are providing trophic support, maintaining communication between neuronal populations, myelination of axons, participating in blood-barrier formation, and regulating the immune response. The immune response of the brain is initiated mainly by astrocytes and microglia. In addition to that, meningeal lymphatic vasculature of the brain augments the immune response. Activated astrocytes and microglia undergo a morphological change that allows them the release number of inflammatory mediators and cytokines. Secretion of cytokines and chemokines attracts blood-derived monocytes and other adaptive immune system members such as T-cells into the inflamed area and they are together with the resident astrocytes and microglia elevate the immune response to a different level.

CCR2 is a chemokine receptor that is expressed in astrocytes, macrophages, endothelial cells, and microglia (Singh, Anshita, and Ravichandiran 2021). CCL2 is the ligand of CCR2. CCR2 activation increases the number of inflammatory cells, TH2 cell differentiation, and CCL2 accumulation (Singh, Anshita, and Ravichandiran 2021). In

this study, we found that CCL2 expression in the *Neu1*$^{-/-}$, *Neu3*$^{-/-}$, and *Neu1*$^{-/-}$ *Neu3*$^{-/-}$ mice compared to WT mice was elevated in the cortex and cerebellum (Figure 3.3). Remarkably, in the cerebellum, the highest increase in the CCL2 expression compared to WT mice was in *Neu1*$^{-/-}$ *Neu3*$^{-/-}$ mice, although *Neu1*$^{-/-}$ and *Neu3*$^{-/-}$ mice showed a significant increase compared to WT mice, too. It is worth noticing that the general expression of CCL2 was much higher in the cerebellum when compared to the cortex.

CCL3 is the ligand of CCR1 and CCR5 and its presence is related to the infiltration of the immune cells. *Neu1*$^{-/-}$, and *Neu1*$^{-/-}$ *Neu3*$^{-/-}$ mice showed a remarkable increase in the cortical CCL3 expression compared to WT mice (Figure 3.4). However, CCL3 expression in the cerebellum of *Neu1*$^{-/-}$ mice showed almost no change when compared to WT mice. The highest CCL3 expression in the cerebellum was shown by *Neu1*$^{-/-}$ *Neu3*$^{-/-}$ mice. Additionally, the overall expression of CCL3 was higher in the cerebellum when compared to the cortex.

CCL5 is an inflammatory cytokine that also participates in homeostatic processes such as oligodendrocyte proliferation, glutamate release from neurons, and neuronal/glial cell communication (Lanfranco et al. 2017). The expression of CCL5 is highly localized in certain brain sections such as white matter (Lanfranco et al. 2017). CCL5 expression in the cortex region was highest in WT mice, and gradually decreased in *Neu1*$^{-/-}$, *Neu3*$^{-/-}$, and *Neu1*$^{-/-}$ *Neu3*$^{-/-}$ mice, where the lowest expression was observed in *Neu1*$^{-/-}$ *Neu3*$^{-/-}$ mice (Figure 3.5). The decrease might be stemming from the homeostatic functions of CCL5 since it also participates in oligodendrocyte proliferation and neuronal communication. The decrease of neuronal population in *Neu1*$^{-/-}$ *Neu3*$^{-/-}$ mice further supports this assumption (Figure 3.10). There was a significant increase in CCL5 expression of *Neu1*$^{-/-}$, and *Neu1*$^{-/-}$ *Neu3*$^{-/-}$ mice which could promote oligodendrocyte proliferation. The overall CCL5 expression was significantly higher in the cerebellum than that of the cortex. The localization of CCL5 being mainly in white matter, astrocytes and microglia further support this assumption due to the abundance of glial cells in the cerebellum.

GFAP is expressed from activated astrocytes. The expression of GFAP was remarkably increased in *Neu1*$^{-/-}$ *Neu3*$^{-/-}$ mice compared to WT, *Neu1*$^{-/-}$ and *Neu3*$^{-/-}$ mice (Figure 3.6 and 3.7). The same pattern was also observed in the cerebellum. Below the granular layer in the cerebellum white matter and fibrous astrocytes are located. Protrusions from fibrous astrocytes in *Neu1*$^{-/-}$ *Neu3*$^{-/-}$ mice were present in the cerebellum

(Figure 3.7L) which indicates astrocyte stellation upon activation. There was minor stellation present in *Neu1*$^{-/-}$ and *Neu3*$^{-/-}$ mice and no stellation was present in WT mice.

MAG (Siglec-4) is capable of dual action that involves inhibition of axonal growth in adult neurons and promoting axonal growth in embryonic neurons (DeBellard et al. 1996). The transfer of sialic acid residues to MAG is directly related to its activity. The desialylation of GD1a and GT1b residues from MAG inhibits axonal growth by decreasing the binding affinity between MAG and neurons (Collins et al. 1997). On the other hand, sialylation of MAG enhances this affinity and allows MAG to promote axonal growth. RT-PCR experiments revealed little to no change in MAG expression between mouse models. The only significant alteration was a slight decrease in MAG expression in the mouse cortex compared to other mouse models (Figure 3.8). MBP staining revealed similar results (Figure 3.9). Neuraminidase 1, and neuraminidase 3 deficiency, and their combined deficiency complicate the desialylation events, which in turn could lead to MAG-induced axonal growth and myelination. However, the slight decrease in cortical MAG expression in *Neu1*$^{-/-}$ *Neu3*$^{-/-}$ mice requires further investigation since MAG did not decrease in the cerebellum. It might be resulting from the sensitivity of cortical neurons to excess storage in comparison with cerebellar neurons since a decrease in the neuronal population was present in the cortex of *Neu1*$^{-/-}$ *Neu3*$^{-/-}$ mice (Figure 3.10). However, this assumption needs further investigation.

Neuronal density in the mouse cortex, thalamus, and cerebellum was investigated by NeuN staining. The staining revealed that there was not any decrease in the neuronal populations in the deficiency of neuraminidase 1 or neuraminidase 3. However, the combined deficiency of said neuraminidases leads to a substantial decrease in neuronal populations in the cortex, thalamus, and cerebellum (Figure 3.10). The decrease in cortical NeuN intensity of *Neu1*$^{-/-}$ *Neu3*$^{-/-}$ mice was 2 times higher than the decrease in cerebellar NeuN intensity. This data supports that in *Neu1*$^{-/-}$ *Neu3*$^{-/-}$ mice, the cerebellum is more resistant to excess storage than that of in cortex.

Morphological staining revealed mild disruption of Purkinje cell layer in *Neu1*$^{-/-}$ mice in line with the findings of de Geest et al, 2002 and severe disruption in PCL of *Neu1*$^{-/-}$ *Neu3*$^{-/-}$ mice (3.12). In addition to that, there was lysosomal vacuolization present in the cortex of *Neu1*$^{-/-}$ *Neu3*$^{-/-}$ mice (Figure 3.11).

Ganglioside expression in the cortex was examined by TLC (Figure 3.13). *Neu1*$^{-/-}$ *Neu3*$^{-/-}$ mice demonstrated a unique expression of gangliosides. In brains and several organs of sialidosis patients, GM3, and GD3 expression was found (Yoshino et al. 1990;

Seyrantepe et al. 2003). In the cortex of *Neu1*$^{-/-}$ *Neu3*$^{-/-}$ mice, GD3 expression was observed. Expression of GD3 is primarily observed in embryonic brains (Yu et al. 2011). In the literature, there is evidence that there are relationships between GD3 accumulation, autophagosome remodelling, and apoptosis (Garofalo et al. 2015), GD3 accumulation and neurodegenerative stimuli and apoptosis (Copani et al. 2002). All of this evidence indicates the presence of a neuroinflammatory environment in a combined deficiency of neuraminidases 1 and 3.

# CHAPTER 5

# CONCLUSION

In this study, neuroinflammation in *Neu1*$^{-/-}$ and *Neu1*$^{-/-}$ *Neu3*$^{-/-}$ mice was shown for the first time through biological, immunohistochemical, chromatographic, and histologic methods. Combined deficiency of neuraminidase 1 and neuraminidase 3 revealed increased expression of inflammatory cytokines in several regions of the mouse brain and a unique expression of gangliosides in the mouse cortex. However, to unravel the exact mechanism of neuroinflammation, more research is necessary.

There are eight different neuronal populations throughout the brain which are: Golgi cells, granule cells, basket cells, stellate cells, Lugaro cells, unipolar brush cells, and candelabrum cells (Revuelta et al. 2020). And the glial subtypes are oligodendrocytes, fibrous astrocytes, protoplasmic (velate) astrocytes, Bergman's glia, and their subset Fañanas cells (feathered cells of Fañanas) (Revuelta et al. 2020). Each neuronal and glial population in the brain responds to neuroinflammatory stimuli differently. And also, the dynamic glycome at their cell surface could alter during morphological change upon activation. Therefore, the neuronal and glial subtypes must be examined individually. For example, the velate astrocytes in the cerebellar granular layer are structurally very different than the fibrous astrocytes within the white matter. Which glial cell and neuronal cell types contribute to inflammation must be investigated.

Neuronal loss was observed in *Neu1*$^{-/-}$ *Neu3*$^{-/-}$ mice and GD3 accumulation was present in the cortex. This data suggests that there is some form of programmed cell death or innate immune system involvement that leads to the death of neurons. Since it is known that dying neurons release DAMPs that activate a variety of immune mechanisms, this assumption must be further elucidated. Whether programmed cell death mechanisms or innate immune system-driven caspase activation leads to cell death and chronic neuroinflammation provides a key to unraveling the inflammatory mechanism.

# REFERENCES


2014. Allen Mouse Brain Atlas. edited by Allen Institute for Brain Science.

Amith, S. R., P. Jayanth, S. Franchuk, S. Siddiqui, V. Seyrantepe, K. Gee, S. Basta, R. Beyaert, A. V. Pshezhetsky, and M. R. Szewczuk. 2009. "Dependence of pathogen molecule-induced Toll-like receptor activation and cell function on Neu1 sialidase." *Glycoconjugate Journal* 26 (9):1197-1212. doi: 10.1007/s10719-009-9239-8.

Archer, L. D., K. J. Langford-Smith, B. W. Bigger, and J. E. Fildes. 2014. "Mucopolysaccharide diseases: a complex interplay between neuroinflammation, microglial activation and adaptive immunity." *J Inherit Metab Dis* 37 (1):1-12. doi: 10.1007/s10545-013-9613-3.

Bhavanandan, Veer P., and D. Channe Gowda. 2014. "Introduction to the Complexity of Cell Surface and Tissue Matrix Glycoconjugates." In *Glycobiology of the Nervous System*, edited by Robert K. Yu and Cara-Lynne Schengrund, 1-31. New York, NY: Springer New York.

Bocquet, O., D. Tembely, D. Rioult, C. Terryn, B. Romier, A. Bennasroune, S. Blaise, H. Sartelet, L. Martiny, L. Duca, and P. Maurice. 2021. "Characterization of novel interactions with membrane NEU1 highlights new regulatory functions for the Elastin Receptor Complex in monocyte interaction with endothelial cells." *Cell and Bioscience* 11 (1). doi: 10.1186/s13578-021-00718-x.

Bosch, Megan E., and Tammy Kielian. 2015. "Neuroinflammatory paradigms in lysosomal storage diseases." *Frontiers in Neuroscience* 9. doi: 10.3389/fnins.2015.00417.

Brandley, B. K., and R. L. Schnaar. 1986. "Cell-surface carbohydrates in cell recognition and response." *J Leukoc Biol* 40 (1):97-111. doi: 10.1002/jlb.40.1.97.

Chan, W. Y., S. Kohsaka, and P. Rezaie. 2007. "The origin and cell lineage of microglia: new concepts." *Brain Res Rev* 53 (2):344-54. doi: 10.1016/j.brainresrev.2006.11.002.

Collins, B. E., L. J. Yang, G. Mukhopadhyay, M. T. Filbin, M. Kiso, A. Hasegawa, and R. L. Schnaar. 1997. "Sialic acid specificity of myelin-associated glycoprotein binding." *J Biol Chem* 272 (2):1248-55. doi: 10.1074/jbc.272.2.1248.

Copani, A., D. Melchiorri, A. Caricasole, F. Martini, P. Sale, R. Carnevale, R. Gradini, M. A. Sortino, L. Lenti, R. De Maria, and F. Nicoletti. 2002. "Beta-amyloid-induced synthesis of the ganglioside GD3 is a requisite for cell cycle

reactivation and apoptosis in neurons." *J Neurosci* 22 (10):3963-8. doi: 10.1523/jneurosci.22-10-03963.2002.

Crocker, P. R., J. C. Paulson, and A. Varki. 2007. "Siglecs and their roles in the immune system." *Nat Rev Immunol* 7 (4):255-66. doi: 10.1038/nri2056.

das Neves, Sofia Pereira, Nickoleta Delivanoglou, and Sandro Da Mesquita. 2021. "CNS-Draining Meningeal Lymphatic Vasculature: Roles, Conundrums and Future Challenges." *Frontiers in Pharmacology* 12. doi: 10.3389/fphar.2021.655052.

de Geest, Natalie, Erik Bonten, Linda Mann, Jean de Sousa-Hitzler, Christopher Hahn, and Alessandra d'Azzo. 2002. "Systemic and neurologic abnormalities distinguish the lysosomal disorders sialidosis and galactosialidosis in mice." *Human Molecular Genetics* 11 (12):1455-1464. doi: 10.1093/hmg/11.12.1455.

DeBellard, M. E., S. Tang, G. Mukhopadhyay, Y. J. Shen, and M. T. Filbin. 1996. "Myelin-associated glycoprotein inhibits axonal regeneration from a variety of neurons via interaction with a sialoglycoprotein." *Mol Cell Neurosci* 7 (2):89-101. doi: 10.1006/mcne.1996.0007.

Demir, S. A., Z. K. Timur, N. Ates, L. A. Martinez, and V. Seyrantepe. 2020. "GM2 ganglioside accumulation causes neuroinflammation and behavioral alterations in a mouse model of early onset Tay-Sachs disease." *Journal of Neuroinflammation* 17 (1). doi: 10.1186/s12974-020-01947-6.

Di Vito, Anna, Giuseppe Donato, and Daniele Tomassoni. 2017. "Molecular and Cellular Mechanisms of Neuroinflammation." *BioMed research international* 2017:8417183-8417183. doi: 10.1155/2017/8417183.

DiSabato, D. J., N. Quan, and J. P. Godbout. 2016. "Neuroinflammation: the devil is in the details." *J Neurochem* 139 Suppl 2:136-153. doi: 10.1111/jnc.13607.

Futerman, Anthony H., and Gerrit van Meer. 2004. "The cell biology of lysosomal storage disorders." *Nature Reviews Molecular Cell Biology* 5 (7):554-565. doi: 10.1038/nrm1423.

Garcia-Dominguez, D. J., N. Hajji, R. Lopez-Alemany, S. Sanchez-Molina, E. Figuerola-Bou, F. J. M. Civanto, S. Rello-Varona, E. Andres-Leon, A. Benito, H. C. Keun, J. Mora, O. M. Tirado, E. de Alava, and L. Hontecillas-Prieto. 2022. "Selective histone methyltransferase G9a inhibition reduces metastatic development of Ewing sarcoma through the epigenetic regulation of NEU1." *Oncogene* 41 (18):2638-2650. doi: 10.1038/s41388-022-02279-w.

Garofalo, T., V. Manganelli, M. Grasso, V. Mattei, A. Ferri, R. Misasi, and M. Sorice. 2015. "Role of mitochondrial raft-like microdomains in the regulation of cell apoptosis." *Apoptosis* 20 (5):621-34. doi: 10.1007/s10495-015-1100-x.

Hanke, M. L., and T. Kielian. 2011. "Toll-like receptors in health and disease in the brain: mechanisms and therapeutic potential." *Clin Sci (Lond)* 121 (9):367-87. doi: 10.1042/cs20110164.

Harris, Julie A., Stefan Mihalas, Karla E. Hirokawa, Jennifer D. Whitesell, Hannah Choi, Amy Bernard, Phillip Bohn, Shiella Caldejon, Linzy Casal, Andrew Cho, Aaron Feiner, David Feng, Nathalie Gaudreault, Charles R. Gerfen, Nile Graddis, Peter A. Groblewski, Alex M. Henry, Anh Ho, Robert Howard, Joseph E. Knox, Leonard Kuan, Xiuli Kuang, Jerome Lecoq, Phil Lesnar, Yaoyao Li, Jennifer Luviano, Stephen McConoughey, Marty T. Mortrud, Maitham Naeemi, Lydia Ng, Seung Wook Oh, Benjamin Ouellette, Elise Shen, Staci A. Sorensen, Wayne Wakeman, Quanxin Wang, Yun Wang, Ali Williford, John W. Phillips, Allan R. Jones, Christof Koch, and Hongkui Zeng. 2019. "Hierarchical organization of cortical and thalamic connectivity." *Nature* 575 (7781):195-202. doi: 10.1038/s41586-019-1716-z.

Hasegawa, T., C. Feijoo Carnero, T. Wada, Y. Itoyama, and T. Miyagi. 2001. "Differential expression of three sialidase genes in rat development." *Biochem Biophys Res Commun* 280 (3):726-32. doi: 10.1006/bbrc.2000.4186.

Jin, Jing, Fuquan Fang, Wei Gao, Hanjian Chen, Jiali Wen, Xuehua Wen, and Junfa Chen. 2021. "The Structure and Function of the Glycocalyx and Its Connection With Blood-Brain Barrier." *Frontiers in Cellular Neuroscience* 15.

Kolter, T., R. L. Proia, and K. Sandhoff. 2002. "Combinatorial ganglioside biosynthesis." *J Biol Chem* 277 (29):25859-62. doi: 10.1074/jbc.R200001200.

Kopitz, J. 2017. "Lipid glycosylation: a primer for histochemists and cell biologists." *Histochem Cell Biol* 147 (2):175-198. doi: 10.1007/s00418-016-1518-4.

Landolfi, N. F., J. Leone, J. E. Womack, and R. G. Cook. 1985. "Activation of T lymphocytes results in an increase in H-2-encoded neuraminidase." *Immunogenetics* 22 (2):159-67. doi: 10.1007/bf00563513.

Lanfranco, M. F., I. Mocchetti, M. P. Burns, and S. Villapol. 2017. "Glial- and Neuronal-Specific Expression of CCL5 mRNA in the Rat Brain." *Front Neuroanat* 11:137. doi: 10.3389/fnana.2017.00137.

Lee, K. M., and A. G. MacLean. 2015. "New advances on glial activation in health and disease." *World J Virol* 4 (2):42-55. doi: 10.5501/wjv.v4.i2.42.

Lein, Ed S., Michael J. Hawrylycz, Nancy Ao, Mikael Ayres, Amy Bensinger, Amy Bernard, Andrew F. Boe, Mark S. Boguski, Kevin S. Brockway, Emi J. Byrnes, Lin Chen, Li Chen, Tsuey-Ming Chen, Mei Chi Chin, Jimmy Chong, Brian E. Crook, Aneta Czaplinska, Chinh N. Dang, Suvro Datta, Nick R. Dee, Aimee L. Desaki, Tsega Desta, Ellen Diep, Tim A. Dolbeare, Matthew J. Donelan, Hong-Wei Dong, Jennifer G. Dougherty, Ben J. Duncan, Amanda J. Ebbert, Gregor

Eichele, Lili K. Estin, Casey Faber, Benjamin A. Facer, Rick Fields, Shanna R. Fischer, Tim P. Fliss, Cliff Frensley, Sabrina N. Gates, Katie J. Glattfelder, Kevin R. Halverson, Matthew R. Hart, John G. Hohmann, Maureen P. Howell, Darren P. Jeung, Rebecca A. Johnson, Patrick T. Karr, Reena Kawal, Jolene M. Kidney, Rachel H. Knapik, Chihchau L. Kuan, James H. Lake, Annabel R. Laramee, Kirk D. Larsen, Christopher Lau, Tracy A. Lemon, Agnes J. Liang, Ying Liu, Lon T. Luong, Jesse Michaels, Judith J. Morgan, Rebecca J. Morgan, Marty T. Mortrud, Nerick F. Mosqueda, Lydia L. Ng, Randy Ng, Geralyn J. Orta, Caroline C. Overly, Tu H. Pak, Sheana E. Parry, Sayan D. Pathak, Owen C. Pearson, Ralph B. Puchalski, Zackery L. Riley, Hannah R. Rockett, Stephen A. Rowland, Joshua J. Royall, Marcos J. Ruiz, Nadia R. Sarno, Katherine Schaffnit, Nadiya V. Shapovalova, Taz Sivisay, Clifford R. Slaughterbeck, Simon C. Smith, Kimberly A. Smith, Bryan I. Smith, Andy J. Sodt, Nick N. Stewart, Kenda-Ruth Stumpf, Susan M. Sunkin, Madhavi Sutram, Angelene Tam, Carey D. Teemer, Christina Thaller, Carol L. Thompson, Lee R. Varnam, Axel Visel, Ray M. Whitlock, Paul E. Wohnoutka, Crissa K. Wolkey, Victoria Y. Wong, Matthew Wood, Murat B. Yaylaoglu, Rob C. Young, Brian L. Youngstrom, Xu Feng Yuan, Bin Zhang, Theresa A. Zwingman, and Allan R. Jones. 2007. "Genome-wide atlas of gene expression in the adult mouse brain." *Nature* 445 (7124):168-176. doi: 10.1038/nature05453.

Li, S. C., Y. T. Li, S. Moriya, and T. Miyagi. 2001. "Degradation of G(M1) and G(M2) by mammalian sialidases." *Biochem J* 360 (Pt 1):233-7. doi: 10.1042/0264-6021:3600233.

Liang, F., V. Seyrantepe, K. Landry, R. Ahmad, A. Ahmad, N. M. Stamatos, and A. V. Pshezhetsky. 2006. "Monocyte differentiation up-regulates the expression of the lysosomal sialidase, Neu1, and triggers its targeting to the plasma membrane via major histocompatibility complex class II-positive compartments." *Journal of Biological Chemistry* 281 (37):27526-27538. doi: 10.1074/jbc.M605633200.

Lipnicanova, S., D. Chmelova, M. Ondrejovic, V. Frecer, and S. Miertus. 2020. "Diversity of sialidases found in the human body - A review." *International Journal of Biological Macromolecules* 148:857-868. doi: 10.1016/j.ijbiomac.2020.01.123.

Lukong, K. E., V. Seyrantepe, K. Landry, S. Trudel, A. Ahmad, W. A. Gahl, S. Lefrancois, C. R. Morales, and A. V. Pshezhetsky. 2001. "Intracellular distribution of lysosomal sialidase is controlled by the internalization signal in its cytoplasmic tail." *Journal of Biological Chemistry* 276 (49):46172-46181. doi: 10.1074/jbc.M104547200.

Lv, T., H. Lv, J. J. Fei, Y. J. Xie, D. Q. Lian, J. Hu, L. Z. Tang, X. D. Shi, J. L. Wang, S. B. Zhang, F. T. Li, X. J. Jiang, and Y. Yi. 2020. "p53-R273H promotes cancer cell migration via upregulation of neuraminidase-1." *Journal of Cancer* 11 (23):6874-6882. doi: 10.7150/jca.44718.

Lyman, M., D. G. Lloyd, X. Ji, M. P. Vizcaychipi, and D. Ma. 2014. "Neuroinflammation: the role and consequences." *Neurosci Res* 79:1-12. doi: 10.1016/j.neures.2013.10.004.

Martins, Carla, Helena Hůlková, Larbi Dridi, Virginie Dormoy-Raclet, Lubov Grigoryeva, Yoo Choi, Alexander Langford-Smith, Fiona L. Wilkinson, Kazuhiro Ohmi, Graziella DiCristo, Edith Hamel, Jerôme Ausseil, David Cheillan, Alain Moreau, Eva Svobodová, Zuzana Hájková, Markéta Tesařová, Hana Hansíková, Brian W. Bigger, Martin Hrebícek, and Alexey V. Pshezhetsky. 2015. "Neuroinflammation, mitochondrial defects and neurodegeneration in mucopolysaccharidosis III type C mouse model." *Brain* 138 (2):336-355. doi: 10.1093/brain/awu355.

McGeer, P. L., and E. G. McGeer. 1995. "The inflammatory response system of brain: Implications for therapy of Alzheimer and other neurodegenerative diseases." *Brain Research Reviews* 21 (2):195-218. doi: 10.1016/0165-0173(95)00011-9.

Meares, Gordon P., and Etty N. Benveniste. 2014. "Inflammation and the Pathophysiology of Astrocytes in Neurodegenerative Diseases." In *Neuroinflammation and Neurodegeneration*, edited by Phillip K. Peterson and Michal Toborek, 61-80. New York, NY: Springer New York.

Meikle, P. J., J. J. Hopwood, A. E. Clague, and W. F. Carey. 1999. "Prevalence of lysosomal storage disorders." *Jama* 281 (3):249-54. doi: 10.1001/jama.281.3.249.

Miyagi, T., K. Takahashi, K. Yamamoto, K. Shiozaki, and K. Yamaguchi. 2018. "Biological and Pathological Roles of Ganglioside Sialidases." In *Gangliosides in Health and Disease*, edited by R. L. Schnaar and P. H. H. Lopez, 121-150.

Miyagi, Taeko, and Kazunori Yamaguchi. 2012. "Mammalian sialidases: Physiological and pathological roles in cellular functions." *Glycobiology* 22 (7):880-896. doi: 10.1093/glycob/cws057.

Monti, E., E. Bonten, A. D'Azzo, R. Bresciani, B. Venerando, G. Borsani, R. Schauer, and G. Tettamanti. 2010. "Sialidases in vertebrates: a family of enzymes tailored for several cell functions." *Adv Carbohydr Chem Biochem* 64:403-79. doi: 10.1016/S0065-2318(10)64007-3.

Möckl, Leonhard. 2020. "The Emerging Role of the Mammalian Glycocalyx in Functional Membrane Organization and Immune System Regulation." *Frontiers in Cell and Developmental Biology* 8.

Nan, X., I. Carubelli, and N. M. Stamatos. 2007. "Sialidase expression in activated human T lymphocytes influences production of IFN-gamma." *J Leukoc Biol* 81 (1):284-96. doi: 10.1189/jlb.1105692.

Ngamukote, S., M. Yanagisawa, T. Ariga, S. Ando, and R. K. Yu. 2007. "Developmental changes of glycosphingolipids and expression of glycogenes in mouse brains." *J Neurochem* 103 (6):2327-41. doi: 10.1111/j.1471-4159.2007.04910.x.

O'Brien, J. S. 1975. "Molecular genetics of GM1 beta-galactosidase." *Clin Genet* 8 (5):303-13.

Oh, Seung Wook, Julie A. Harris, Lydia Ng, Brent Winslow, Nicholas Cain, Stefan Mihalas, Quanxin Wang, Chris Lau, Leonard Kuan, Alex M. Henry, Marty T. Mortrud, Benjamin Ouellette, Thuc Nghi Nguyen, Staci A. Sorensen, Clifford R. Slaughterbeck, Wayne Wakeman, Yang Li, David Feng, Anh Ho, Eric Nicholas, Karla E. Hirokawa, Phillip Bohn, Kevin M. Joines, Hanchuan Peng, Michael J. Hawrylycz, John W. Phillips, John G. Hohmann, Paul Wohnoutka, Charles R. Gerfen, Christof Koch, Amy Bernard, Chinh Dang, Allan R. Jones, and Hongkui Zeng. 2014. "A mesoscale connectome of the mouse brain." *Nature* 508 (7495):207-214. doi: 10.1038/nature13186.

Ohmi, Kazuhiro, David S. Greenberg, Kavitha S. Rajavel, Sergey Ryazantsev, Hong Hua Li, and Elizabeth F. Neufeld. 2003. "Activated microglia in cortex of mouse models of mucopolysaccharidoses I and IIIB." *Proceedings of the National Academy of Sciences* 100 (4):1902-1907. doi: doi:10.1073/pnas.252784899.

Pereira, V. G., M. L. Gazarini, L. C. Rodrigues, F. H. da Silva, S. W. Han, A. M. Martins, I. L. Tersariol, and V. D'Almeida. 2010. "Evidence of lysosomal membrane permeabilization in mucopolysaccharidosis type I: rupture of calcium and proton homeostasis." *J Cell Physiol* 223 (2):335-42. doi: 10.1002/jcp.22039.

Platt, F. M., B. Boland, and A. C. van der Spoel. 2012. "The cell biology of disease: lysosomal storage disorders: the cellular impact of lysosomal dysfunction." *J Cell Biol* 199 (5):723-34. doi: 10.1083/jcb.201208152.

Platt, F. M., A. d'Azzo, B. L. Davidson, E. F. Neufeld, and C. J. Tifft. 2018. "Lysosomal storage diseases." *Nat Rev Dis Primers* 4 (1):27. doi: 10.1038/s41572-018-0025-4.

Prinetti, A., V. Chigorno, S. Prioni, N. Loberto, N. Marano, G. Tettamanti, and S. Sonnino. 2001. "Changes in the lipid turnover, composition, and organization, as sphingolipid-enriched membrane domains, in rat cerebellar granule cells developing in vitro." *J Biol Chem* 276 (24):21136-45. doi: 10.1074/jbc.M010666200.

Pshezhetsky, A. V., and M. Ashmarina. 2001. "Lysosomal multienzyme complex: biochemistry, genetics, and molecular pathophysiology." *Prog Nucleic Acid Res Mol Biol* 69:81-114. doi: 10.1016/s0079-6603(01)69045-7.

Pshezhetsky, A. V., and M. Ashmarina. 2018. "Keeping it trim: roles of neuraminidases in CNS function." *Glycoconjugate Journal* 35 (4):375-386. doi: 10.1007/s10719-018-9837-4.

Puchwein-Schwepcke, Alexandra, Orsolya Genzel-Boroviczény, and Claudia Nussbaum. 2021. "The Endothelial Glycocalyx: Physiology and Pathology in Neonates, Infants and Children." *Frontiers in Cell and Developmental Biology* 9. doi: 10.3389/fcell.2021.733557.

Reily, C., T. J. Stewart, M. B. Renfrow, and J. Novak. 2019. "Glycosylation in health and disease." *Nat Rev Nephrol* 15 (6):346-366. doi: 10.1038/s41581-019-0129-4.

Revuelta, M., T. Scheuer, L. J. Chew, and T. Schmitz. 2020. "Glial Factors Regulating White Matter Development and Pathologies of the Cerebellum." *Neurochem Res* 45 (3):643-655. doi: 10.1007/s11064-020-02961-z.

Roitt, I.M., J. Brostoff, and D.K. Male. 2001. *Immunology*: Mosby.

Schnaar, R. L., R. Gerardy-Schahn, and H. Hildebrandt. 2014. "Sialic acids in the brain: gangliosides and polysialic acid in nervous system development, stability, disease, and regeneration." *Physiol Rev* 94 (2):461-518. doi: 10.1152/physrev.00033.2013.

Schnaar, R. L., and T. Kinoshita. 2015. "Glycosphingolipids." In *Essentials of Glycobiology*, edited by A. Varki, R. D. Cummings, J. D. Esko, P. Stanley, G. W. Hart, M. Aebi, A. G. Darvill, T. Kinoshita, N. H. Packer, J. H. Prestegard, R. L. Schnaar and P. H. Seeberger, 125-35. Cold Spring Harbor (NY): Cold Spring Harbor Laboratory Press


Seyrantepe, V., S. A. Demir, Z. K. Timur, J. Von Gerichten, C. Marsching, E. Erdemli, E. Oztas, K. Takahashi, K. Yamaguchi, N. Ates, B. D. Demir, T. Dalkara, K. Erich, C. Hopf, R. Sandhoff, and T. Miyagi. 2018. "Murine Sialidase Neu3 facilitates GM2 degradation and bypass in mouse model of Tay-Sachs disease." *Experimental Neurology* 299:26-41. doi: 10.1016/j.expneurol.2017.09.012.

Seyrantepe, V., A. Hinek, J. Peng, M. Fedjaev, S. Ernest, Y. Kadota, M. Canuel, K. Itoh, C. R. Morales, J. Lavoie, J. Tremblay, and A. V. Pshezhetsky. 2008. "Enzymatic activity of lysosomal carboxypeptidase (cathepsin) a is required for proper elastic fiber formation and inactivation of endothelin-1." *Circulation* 117 (15):1973-1981. doi: 10.1161/circulationaha.107.733212.

Seyrantepe, V., A. Iannello, F. Liang, E. Kanshin, P. Jayanth, S. Samarani, M. R. Szewczuk, A. Ahmad, and A. V. Pshezhetsky. 2010. "Regulation of

Phagocytosis in Macrophages by Neuraminidase 1." *Journal of Biological Chemistry* 285 (1):206-215. doi: 10.1074/jbc.M109.055475.

Seyrantepe, V., K. Landry, S. Trudel, J. A. Hassan, C. R. Morales, and A. V. Pshezhetsky. 2004. "Neu4, a novel human lysosomal lumen sialidase, confers normal phenotype to sialidosis and galactosialidosis cells." *Journal of Biological Chemistry* 279 (35):37021-37029. doi: 10.1074/jbc.M404531200.

Seyrantepe, V., H. Poulpetova, R. Froissart, M. T. Zabot, I. Marie, and A. V. Pshezhetsky. 2003. "Molecular pathology of NEU1 gene in sialidosis." *Human Mutation* 22 (5):343-352. doi: 10.1002/humu.10268.

Singer, S. J., and G. L. Nicolson. 1972. "The fluid mosaic model of the structure of cell membranes." *Science* 175 (4023):720-31. doi: 10.1126/science.175.4023.720.

Singh, S., D. Anshita, and V. Ravichandiran. 2021. "MCP-1: Function, regulation, and involvement in disease." *Int Immunopharmacol* 101 (Pt B):107598. doi: 10.1016/j.intimp.2021.107598.

Sipione, S., J. Monyror, D. Galleguillos, N. Steinberg, and V. Kadam. 2020. "Gangliosides in the Brain: Physiology, Pathophysiology and Therapeutic Applications." *Front Neurosci* 14:572965. doi: 10.3389/fnins.2020.572965.

Stamatos, N. M., I. Carubelli, D. van de Vlekkert, E. J. Bonten, N. Papini, C. Feng, B. Venerando, A. d'Azzo, A. S. Cross, L. X. Wang, and P. J. Gomatos. 2010. "LPS-induced cytokine production in human dendritic cells is regulated by sialidase activity." *J Leukoc Biol* 88 (6):1227-39. doi: 10.1189/jlb.1209776.

Starcher, B., A. d'Azzo, P. W. Keller, G. K. Rao, D. Nadarajah, and A. Hinek. 2008. "Neuraminidase-1 is required for the normal assembly of elastic fibers." *Am J Physiol Lung Cell Mol Physiol* 295 (4):L637-47. doi: 10.1152/ajplung.90346.2008.

Suzuki, A. 2006. "Genetic basis for the lack of N-glycolylneuraminic acid expression in human tissues and its implication to human evolution." *Proc Jpn Acad Ser B Phys Biol Sci* 82 (3):93-103. doi: 10.2183/pjab.82.93.

Tettamanti, G. 2004. "Ganglioside/glycosphingolipid turnover: new concepts." *Glycoconj J* 20 (5):301-17. doi: 10.1023/B:GLYC.0000033627.02765.cc.

Timur, Z. K., S. A. Demir, and V. Seyrantepe. 2016. "Lysosomal Cathepsin A Plays a Significant Role in the Processing of Endogenous Bioactive Peptides." *Frontiers in Molecular Biosciences* 3. doi: 10.3389/fmolb.2016.00068.

Uemura, T., K. Shiozaki, K. Yamaguchi, S. Miyazaki, S. Satomi, K. Kato, H. Sakuraba, and T. Miyagi. 2009. "Contribution of sialidase NEU1 to suppression of

metastasis of human colon cancer cells through desialylation of integrin beta4." *Oncogene* 28 (9):1218-29. doi: 10.1038/onc.2008.471.

Varki, A., and R. Schauer. 2009. "Sialic Acids." In *Essentials of Glycobiology*, edited by A. Varki, R. D. Cummings, J. D. Esko, H. H. Freeze, P. Stanley, C. R. Bertozzi, G. W. Hart and M. E. Etzler. Cold Spring Harbor (NY): Cold Spring Harbor Laboratory Press


Wang, Jing, and Robert K. Yu. 2013. "Interaction of ganglioside GD3 with an EGF receptor sustains the self-renewal ability of mouse neural stem cells in vitro." *Proceedings of the National Academy of Sciences* 110 (47):19137-19142. doi: doi:10.1073/pnas.1307224110.

Wilkinson, Fiona L., Rebecca J. Holley, Kia J. Langford-Smith, Soumya Badrinath, Aiyin Liao, Alex Langford-Smith, Jonathan D. Cooper, Simon A. Jones, J. Ed Wraith, Rob F. Wynn, Catherine L. R. Merry, and Brian W. Bigger. 2012. "Neuropathology in Mouse Models of Mucopolysaccharidosis Type I, IIIA and IIIB." *PLOS ONE* 7 (4):e35787. doi: 10.1371/journal.pone.0035787.

Yamaguchi, K., K. Hata, K. Koseki, K. Shiozaki, H. Akita, T. Wada, S. Moriya, and T. Miyagi. 2005. "Evidence for mitochondrial localization of a novel human sialidase (NEU4)." *Biochem J* 390 (Pt 1):85-93. doi: 10.1042/bj20050017.

Yamaguchi, K., K. Shiozaki, S. Moriya, K. Koseki, T. Wada, H. Tateno, I. Sato, M. Asano, Y. Iwakura, and T. Miyagi. 2012. "Reduced susceptibility to colitis-associated colon carcinogenesis in mice lacking plasma membrane-associated sialidase." *PLoS One* 7 (7):e41132. doi: 10.1371/journal.pone.0041132.

Yang, L. J., C. B. Zeller, N. L. Shaper, M. Kiso, A. Hasegawa, R. E. Shapiro, and R. L. Schnaar. 1996. "Gangliosides are neuronal ligands for myelin-associated glycoprotein." *Proc Natl Acad Sci U S A* 93 (2):814-8. doi: 10.1073/pnas.93.2.814.

Yoshino, Hiide, Kotaro Miyashita, Nobuyuki Miyatani, Toshio Ariga, Yasuhiro Hashimoto, Shoji Tsuji, Kiyomitsu Oyanagi, Eisaku Ohama, Fusahiro Ikuta, Akemi Suzuki, and Tadashi Miyatake. 1990. "Abnormal glycosphingolipid metabolism in the nervous system of galactosialidosis." *Journal of the Neurological Sciences* 97 (1):53-65. doi: https://doi.org/10.1016/0022-510X(90)90098-8.

Yu, R. K., L. J. Macala, T. Taki, H. M. Weinfield, and F. S. Yu. 1988. "Developmental changes in ganglioside composition and synthesis in embryonic rat brain." *J Neurochem* 50 (6):1825-9. doi: 10.1111/j.1471-4159.1988.tb02484.x.

Yu, Robert K., Yi-Tzang Tsai, Toshio Ariga, and Makoto Yanagisawa. 2011. "Structures, biosynthesis, and functions of gangliosides--an overview." *Journal of oleo science* 60 (10):537-544. doi: 10.5650/jos.60.537.

Yuziuk, J. A., C. Bertoni, T. Beccari, A. Orlacchio, Y. Y. Wu, S. C. Li, and Y. T. Li. 1998. "Specificity of mouse GM2 activator protein and beta-N-acetylhexosaminidases A and B. Similarities and differences with their human counterparts in the catabolism of GM2." *J Biol Chem* 273 (1):66-72. doi: 10.1074/jbc.273.1.66.